AD

Novel Robust Models for Damage Tolerant Helicopter Components

FINAL TECHNICAL REPORT

by

M Lang, P E Irving, C Stolz, V Zitounis

October 2001 - December 2002

EADS Military Aircraft, Munich, Germany
Cranfield University, UK

NRCC Contract No 68171-01-C-9015

Cranfield University Report No. DT 9623/55

Approved for Public Release; distribution unlimited

REPORT DOCUMENTATION PAGE

Form Approved
OMB No. 0704-0188

1. AGENCY USE ONLY (Leave blank)	2. REPORT DATE	3. REPORT TYPE AND DATES COVERED
	December 2002	Final, October 2001-December 2002

4. TITLE AND SUBTITLE
Novel Robust Models for Damage Tolerant Helicopter Components

5. FUNDING NUMBERS
N68171-01-C-9015

6. AUTHOR(S)

M Lang, P E Irving, C Stolz, V Zitounis,

7. PERFORMING ORGANISATION NAME(S) AND ADDRESS(ES)

Cranfield University
Cranfield, Beds
MK43 0AL, UK

EADS
Military Aircraft
D-81663, Munchen, Germany

8. PERFORMING ORGANISATION REPORT NUMBER
DT9623/55

9. SPONSORING/MONITORING AGENCY NAME(S) AND ADDRESS(ES)
European Research Office, US Army Research, Development & Standardisation Group,
223-231 Old Marylebone Road, London, NWI, UK

10. SPONSORING/MONITORING AGENCY REPORT NUMBER

11. SUPPLEMENTARY NOTES

12a. DISTRIBUTION/AVAILABILITY STATEMENT

12b. DISTRIBUTION CODE

13. ABSTRACT

A new approach to the prediction of crack growth fatigue lives under variable amplitude loading, the K_{PR} approach, is described. K_{PR} is the minimum stress intensity for crack propagation during a loading cycle and is sensitive to the immediate loading history at the crack tip. Four parameters describe changes in K_{PR} as a function of load history. Unlike other models the K_{PR} model has no fitting parameter.

The four K_{PR} parameters for 7010-T73651 aluminium and SAE 4340 quenched and tempered steel, together with necessary crack growth rate data, were measured. Variable amplitude testing was performed on the same materials under two loading spectra, Rotarix, a standard spectrum for a helicopter rotorhead, and Falstaff, a fixed wing fighter aircraft spectrum. The variable amplitude crack growth data were used to validate the K_{PR} model together with 4 other models for fatigue crack growth. These were FASTRAN, the 3 models within AFGROW, namely, Wheeler, Willenborg and the closure model.

It was found that the K_{PR} model provided the best agreement for Rotarix on 7010 aluminium, with errors of only 15-20%. FASTRAN was second best. All other models made non conservative predictions. On Falstaff, agreement was not as good on aluminium alloys, but K_{PR} was still the most accurate model The K_{PR} model performed not as well on the SAE 4340 steel. For Rotarix. K_{PR} still was the closest, for Falstaff, other models achieved better accuracy. All predictions were made blind, in advance of knowledge of the validation test data.

14. SUBJECT TERMS
Fatigue crack growth, prediction of fatigue lives; damage tolerance; load interaction effects models.

15. NUMBER OF PAGES
65

16. PRICE CODE

17. SECURITY CLASSIFICATION OF REPORT	18. SECURITY CLASSIFICATION OF THIS PAGE	19. SECURITY CLASSIFICATION OF ABSTRACT	20. LIMITATION OF ABSTRACT
Unclassified	Unclassified	Unclassified	UL

ABSTRACT

A new approach to the calculation of crack growth fatigue lives under variable amplitude loading, the K_{PR} approach is described. Details are provided of the principles of the technique, the relevant material parameters and suggested experimental techniques for measurement of the parameters. A description is provided of the basis of a model for calculation of fatigue crack growth rates under variable amplitude loading.

K_{PR} is the minimum stress intensity for crack propagation during a loading cycle and is sensitive to the immediate loading history at the crack tip. Four parameters describe changes in K_{PR} as a function of load history. Once these are known for a given material, the effective ΔK, ΔK_{eff}, at the crack tip at each load cycle can be calculated, and the resultant growth increment derived from knowledge of the relation between crack growth rate da/dN and ΔK_{eff}. Unlike other approaches, the K_{PR} model has no fitting parameter.

Work is described which has measured the four K_{PR} parameters for 7010-T73651 aluminium and SAE 4340 quenched and tempered steel, together with necessary crack growth rate data for the two materials, using a specially developed automated crack growth monitoring system equipped with test machine control. Testing has also been performed on the same materials under two variable amplitude loading spectra, Rotarix, a standard spectrum developed from load measurements on a helicopter rotorhead, and Falstaff, a fixed wing fighter aircraft spectrum. There were 4 variants of the Rotarix spectrum which were used for analysis. The measured lives and crack growth data were used to provide validation test data for the new K_{PR} model and 4 other models for fatigue crack growth, FASTRAN, and 3 models within AFGROW, namely, Wheeler, Willenborg and a closure based model. The resultant lives were compared with predictions on all models.

It was found that the K_{PR} model provided the best agreement with lives for Rotarix spectra on 7010 aluminium, with errors of only 15-20%. This was the most accurate model with FASTRAN second best. All other models made non conservative predictions. On Falstaff, agreement was not as good on aluminium alloys, but K_{PR} was still the most accurate model. The K_{PR} model performed not as well on the SAE 4340 steel. For Rotarix, K_{PR} still was the closest, for Falstaff other models achieved better accuracy. It has to be noted that all predictions were made blind, as the subcontractor EADS Military Aircraft had to provide the predictions upfront.

A full sensitivity study is made of the role of the various parameters in the prediction accuracy of the K_{PR} model, and suggestions are made for the performance of the model under the various material and load history combinations. Suggestions are made for future directions of research in this area.

Keywords

Damage Tolerance, Rotorcraft, Crack Growth Prediction, Crack Growth, Inspection Intervals, Rotarix, Crack Growth Model, Al 7010, SAE 4340

Novel Robust Models for Damage Tolerant Helicopter Components

Final report Dec. 2002

M Lang, P E Irving, C Stolz, V Zitounis

Contents **Page**

Nomenclature

K_{PR}	Minimum stress intensity required for crack growth in a load cycle
ΔK	Stress intensity range
K_{max}	Maximum stress intensity in fatigue cycle
K_{min}	Minimum in fatigue cycle
ΔK_{eff}	Effective $\Delta K = (K_{max} - K_{PR} - \Delta K_T)$
ΔK_{BL}, $K_{max\ BL}$	Range and maximum stress intensities at base level before overload
ΔK_T	Intrinsic threshold stress intensity
$K_{max\ OL}$	Maximum stress intensity at overload
K_{UL}	Minimum stress intensity achieved in half cycle after overload
$K_{max}/K_{max\ OL}$	Overload ratio
$K_{UL}/K_{max\ OL}$	Underload ratio
R	R ratio= K_{min}/K_{max}
K_W	Stress intensity at crack tip at minimum load, accounting for closure
R_{tip}	R ratio experienced by crack tip = K_W/K_{max}
UR	Generalised R ratio parameter UR = R_{tip} for tension, in compression UR = σ_p/σ_y
σ_p	Far field compression stress
σ_y	Proof strength of material

1. Introduction

This final report describes results of research undertaken between November 2001 and December 2002 to determine crack growth properties necessary for the K_{PR} approach and calculation of fatigue crack growth lives under variable amplitude loading using the K_{PR} approach. These results were then compared with the output of traditional models. The research was a collaboration between Cranfield University and EADS Munich, with Cranfield performing the majority of experimental work and EADS performing analytical predictions.

Approach

Fatigue crack growth properties of two materials, 7010-T73651 aluminium, and SAE 4340 quenched and tempered steel will be measured, and used as input to a new model for fatigue crack growth under variable amplitude loading- the K_{PR} approach. The model was used to make predictions of crack growth lives for cracked compact tension samples of the two materials when subjected to a range of variable amplitude load spectra. The predictions will be validated by comparison with measured crack growth lives under identical materials and loads spectra. The differences between prediction and experiment will be assessed in the light of current understanding of variable amplitude fatigue crack growth.

Statement of work

(a) Measurement of constant amplitude fatigue crack growth rates for R constant and K_{max} constant regimes for the two materials. Measurement of fatigue crack growth rates under variable amplitude loading, namely 3 variants of the Rotarix spectrum, Falstaff (these differ from the spectra suggested in the original proposal).

(b) Measurement of material dependent functions necessary for crack growth predictions based on the K_{PR} approach.

(c) Modifications of Software for predictions of fatigue crack growth rates using K_{PR}.

(d) Modelling and analysis to predict fatigue crack growth rates using K_{PR}, AFGROW and FASTRAN models for crack growth prediction.

(e) Analysis of modelling results.

(f) Parameter study for K_{PR}.

(g) Reporting.

Requirements for robust models for fatigue crack growth life predictions

Despite years of development of models for fatigue crack growth under variable amplitude loading and the subsequent development of computer code implementing the models in various forms, their robustness is some way short of ideal. Models frequently contain one or more material, stress state or other constants and fitting parameters which allow the model to be "tuned" to specific materials and or loading spectra to give best possible accuracy. This can be advantageous when dealing with a well established design in a well understood loading environment. Designs in which there have been no previous calculations of crack growth lives in new materials subjected to novel loading spectra or imminent in service problems, require accuracy first time. This is particularly true when considering damage tolerant design of

helicopters. The combination of large numbers of load cycles per flight hour combined with use of high strength materials subjected to high stresses leads to a situation where macroscopic fatigue crack growth occupies a small fraction- perhaps less than a few tens or hundreds of flight hours- of the total life of the part. Under these circumstances errors and uncertainties in crack growth prediction cannot be covered by generous factors of safety. The crack growth lives might be relatively small compared to fixed wing structures. A reliable and robust crack growth model to predict the growth from assumed cracks or flaws would help in gaining confidence in damage tolerance methodology.

Recent work (1, 2, 3) has demonstrated that loading spectra on helicopter rotor and lift frame components are particularly damaging. They consist of large numbers of high R ratio cycles or small range originating in the rotor motion, interspersed with larger range underloads to lower or zero loads. Spectra of this type cause crack acceleration rather than crack retardation relative to linear models without load interaction effects. Traditional models for variable amplitude fatigue crack growth produce non conservative predictions on these spectra.

In the present work, different crack growth models have been compared to assess the robustness of crack growth calculations for rotary wing structures.

The various crack growth prediction models and codes assessed in this project were:

1) Wheeler model (AFGROW version)
2) Willenborg model (AFGROW version)
3) Closure Model (AFGROW version)
4) FASTRAN Model (a closure based model using cycle by cycle calculations)

These models have been compared to

5) The K_{PR}-Model

The K_{PR} model is the most recent development among the above models. It was developed in the last 5 years. The model was previously incorporated into a small software package. The main task of this research is now to use this software to assess the robustness and accuracy of the K_{PR} approach with respect to the other models listed above.

The K_{PR} model will be now briefly described and differences to other models outlined.

2. Crack growth calculation using the K_{PR} approach

2.1 K_{PR} Model

The development and detailed description of the K_{PR} approach is described in (4-8). It is based on a simple criterion, namely crack growth itself. Figure 1 shows the situation that there is an effective fraction of a load cycle range, which drives a fatigue crack and a fraction that does not directly drive the crack. The crucial parameter is K_{PR}, the stress intensity factor above which the crack propagates. Thus ΔK_{eff} can be defined as:

$$\Delta K_{eff} = K_{\max} - K_{PR} - \Delta K_T$$

where K_{max} is the maximum stress intensity of the load cycle and ΔK_T is the intrinsic threshold for fatigue crack propagation at a high R ratio (0.8-0.9) or relatively small crack lengths. The ΔK_{eff} approach thus is analogous to the ΔK_{eff} used in crack closure based models, but the K_{PR} concept is

more generic than crack closure, incorporating modifications in ΔK_{eff} caused by compressive residual stresses ahead of the crack tip (see refs 4, 5, 6).

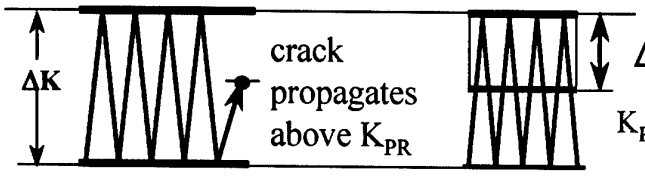

$$\Delta K_{eff} = K_{max} - K_{PR} - \Delta K_T$$

Figure 1

Figure 2 shows the procedure for experimental determination of K_{PR}. In this example the loading is constant amplitude. After constant amplitude cycling, the stress intensity range ΔK is reduced to a value just above ΔK_T, defined as above. If there is no detectable crack growth after 200,000 cycles, the mean K is increased by an increment δ ($\approx$0.2 MPa $m^{1/2}$,) and 2 x 10^5 cycles applied at the new settings. If no crack growth is detected at the new settings the process is repeated, until a K_{max} is attained where growth occurs. K_{PR} is then calculated as:

$$K_{PR} = \frac{K_{maxk} + K_{maxk-1}}{2} - \Delta K_T$$

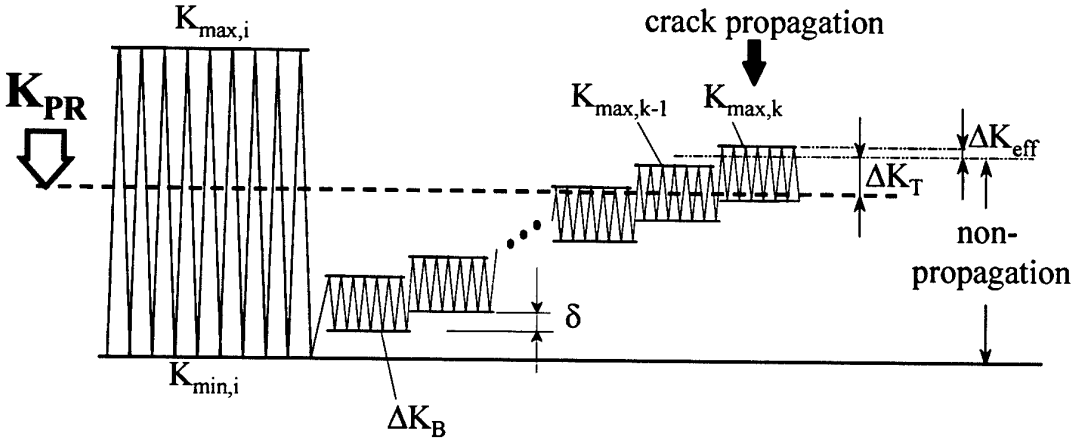

Figure 2

K_{PR} may also be determined after various forms of load transients such as overloads and underloads, by following the same procedures.

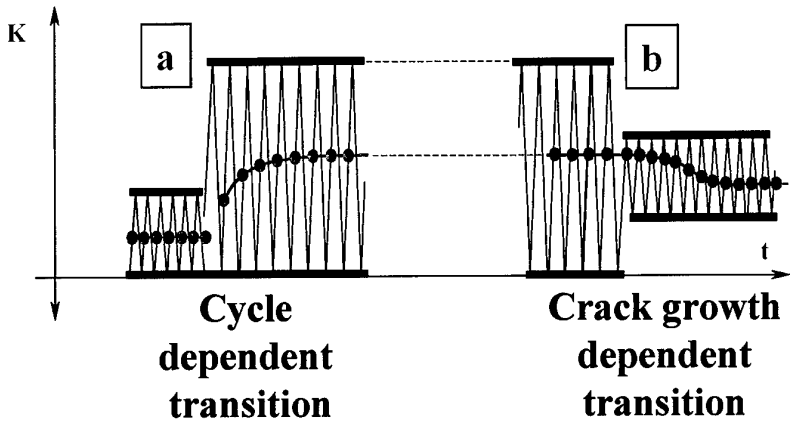

These two fundamentally different cases lead to the integrated K_{PR} approach

Figure 3

The value of K_{PR} is dependent on the previous loading history of the fatigue crack. It has been established (4, 5, 6) that there are two fundamentally different forms of load transitions in crack growth. These are shown in Figure 3.

The K_{PR} theory distinguishes between a cycle dependent transition and a crack growth dependent transition, i.e. between a low – high step and a high – low step in loading. K_{PR} and hence ΔK_{eff} can be determined experimentally and used as the basis for a crack growth prediction model. The crack growth dependent transition is also referred to as the decline curve. The theory, described in detail in (4, 5) says that there are only three types of load cycle:

1) A **Type I Cycle** that dynamically and directly changes K_{PR}. These cycles are those in the cycle dependent transition in Figure 3a.

2) A **Type II Cycle** that does not dynamically change K_{PR}. K_{PR} will gradually change with increasing cycles via crack extension. The maximum K of a Type II cycle exceeds the current K_{PR} value and produces crack growth, but is less than the K_{max} achieved for a type I cycle. Type II cycles are those in the crack growth dependent transition (Figure 3b) and result in the gradual decline of K_{PR} after a Type I cycle.

3) A **Type III Cycle** does not produce crack growth. The maximum K of this cycle does not exceed the current K_{PR} value and is therefore a harmless cycle.

The approach is represented in Figure 4 where the regions of the three types of cycles are indicated in a "Fatigue Crack Growth Map".

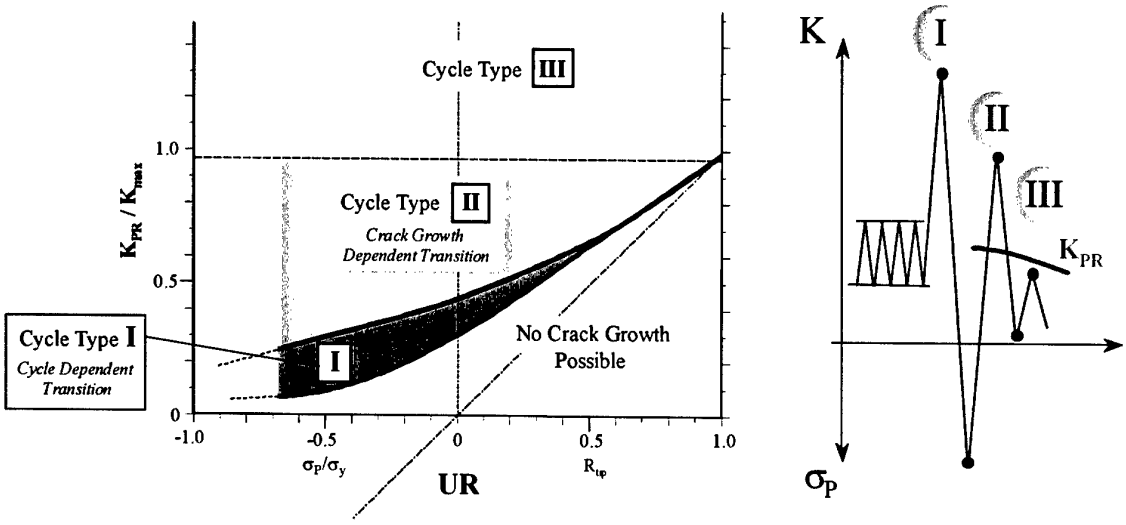

Figure 4

The chart in Figure 4 shows K_{PR}, expressed as a fraction of K_{max} of the transition cycle, plotted against the unloading ratio UR. UR is a general mean stress parameter, valid for both tension and compression load excursions (4-8). For tension excursions, UR= R_{tip}, the R ratio experienced by the crack tip, and is defined as:

$$R_{tip} = K_w/K_{max};$$

where K_w is the stress intensity that is seen by the crack tip at the minimum in the load cycle in case closure is present . K_w is equal to K_{min} for situations with no closure present.

For compression loading, UR is negative and is equal to the compression ratio σ_p/σ_y, whereσ_p is the compressive far field stress, and σ_y is the yield strength of the material. In the current research, loading is confined to tension only.

The two curves in Figure 4 (boundaries to area I) represent data for constant amplitude loading (the upper curve) and a single overload (the lower curve). The region in between these two curves (called master curves) represents data for all Type I cycle dependent transitions. The region for the Type II cycles is between the curve for CA loading and the line $K_{PR}/K_{max} = 1$. The Type III cycles are located above $K_{PR}/K_{max} = 1$.

The interpretation of the three type of cycles with their maximum load in respect to K_{PR} can be seen in the right part of Figure 4.

Using this methodology, it was found in (4, 5) that if we are able to solve the two transitions shown in Figure 3, crack growth prediction is possible without using a fitting factor.

For software modeling of crack growth, Type I cycles have three sub-categories that need to be taken into account. These three cases together with the Type II transition case are shown in Figure 5. In this diagram K values at load turning points are plotted schematically against reversed plastic zone size extent.

Diagram I_1 shows the situation when a new Type I cycle occurs. It establishes a new reference maximum value of K, termed Max I, and a minimum level, Min I. If on a subsequent load increment, an overload occurs, a new upper boundary for Max I is established. If subsequent crack growth is constant amplitude loading, the reference Max I will decline with a function coupled to the decline of K_{PR}. K_{PR} declines to the steady state K_{PR} value (CA-Loading case) of the following Type II cycles. Max I declines to the corresponding maximum load of this "constant amplitude loading" cycle. More details of the quantitative expressions governing the decline of Max I and K_{PR} can be found in (5).

If the minimum load of a subsequent cycle is below the current lower reference level Min I, (Diagram I_2 in Figure 5) the reference level (Min I) is immediately lowered. This can happen in both tensile and compressive regions. Diagrams I_2 in tension and I_3 in compression distinguish between these cases. This is necessary, since the Fatigue Crack Growth Map (Figure 4) separates the tensile regime with an R value of the K factor from the compression ratio σ_p / σ_y.

For the relatively rare case that the minimum of a Type II cycle is above the current K_{PR}, an I_4 cycle is defined, where K_{PR} is set to the value for a single overload. It was shown experimentally that K_{PR} can never be below K_{min}. Since these cycles naturally have a high R-value, the difference between a K_{PR} due to CA-loading and a single overload is very small, as can be seen in Figure 4 (only a small transition takes place).

A Type I cycle sets a new plastic zone that is calculated according to the equation in (4). The calculations are conducted with two times this plastic zone size, since interferometer investigations (7) have shown that the experimentally measured cyclic plastic zone size is about double the Irwin monotonic plastic zone.

A model has been constructed to deduce the appropriate value of K_{PR} for the next load cycle, based on the values of the previous load cycles in a general variable amplitude load sequence. The correct crack growth increment may then be assigned to the load cycle, before assigning a new value of K_{PR} to the next load cycle in turn, taking account of any changes in load conditions.

The model also can deal with block loading. There is a routine included that asks continuously if K_{PR} has reached a steady state value (CA-loading). If the following maximum and minimum is the same as the previous one, the respective steady state K_{PR} value is used to calculate the corresponding crack growth increment. The software moreover has a no - load interaction module and a constant amplitude loading module where the life for loading under a certain R value can be calculated. A flow chart of the software is shown in Figure 6.

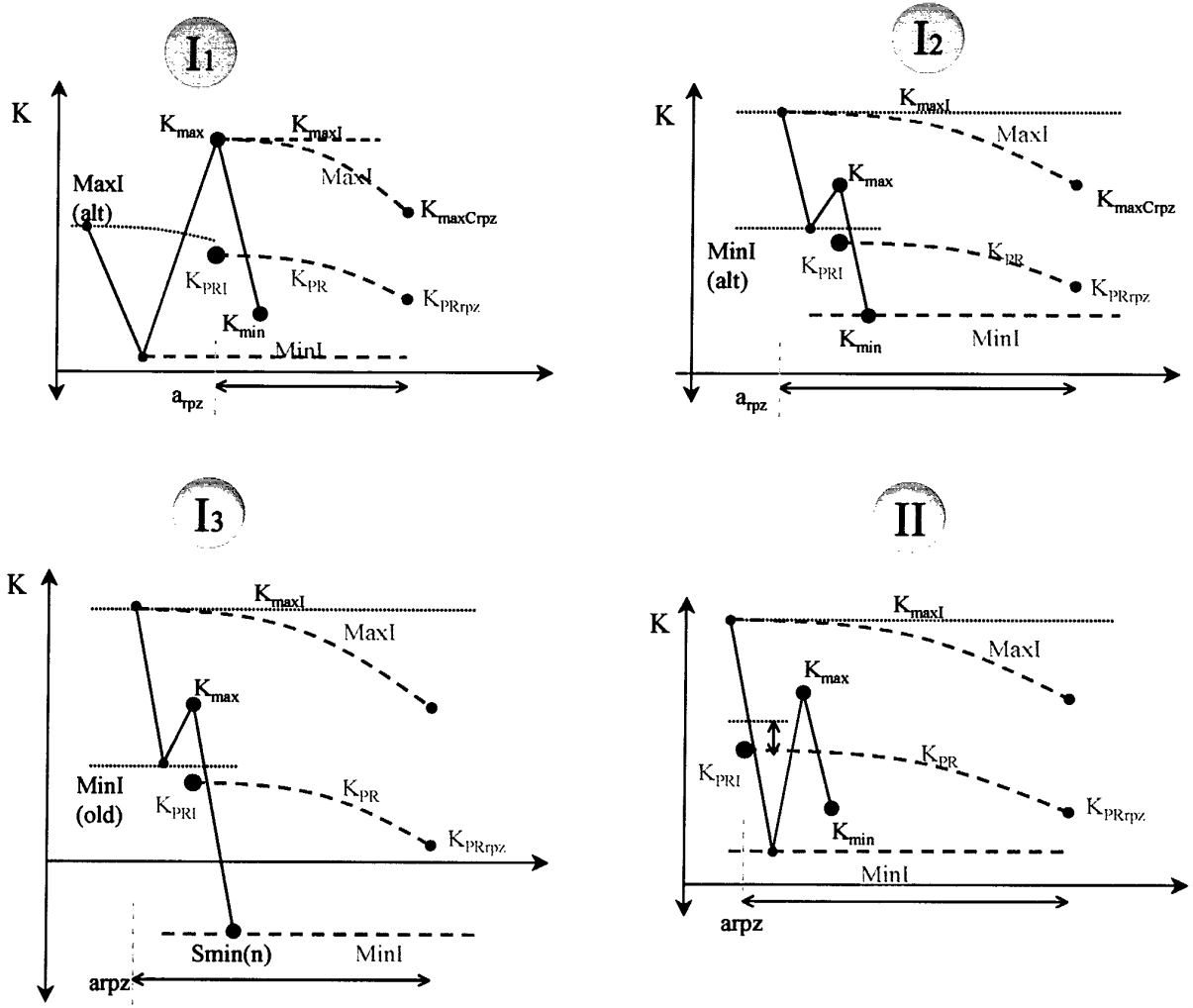
I1
K
Kmax
KmaxI
MaxI
MaxI
(alt)
KmaxCrpz
KPRI
KPR
KPRrpz
Kmin
MinI
arpz
I2
K
KmaxI
MaxI
Kmax
KmaxCrpz
MinI
(alt)
KPRI
KPR
KPRrpz
Kmin
MinI
arpz
I3
K
KmaxI
MaxI
Kmax
MinI
(old)
KPRI
KPR
KPRrpz
Smin(n)
MinI
arpz
II
K
KmaxI
MaxI
Kmax
KPRI
KPR
KPRrpz
Kmin
MinI
arpz

Figure 5

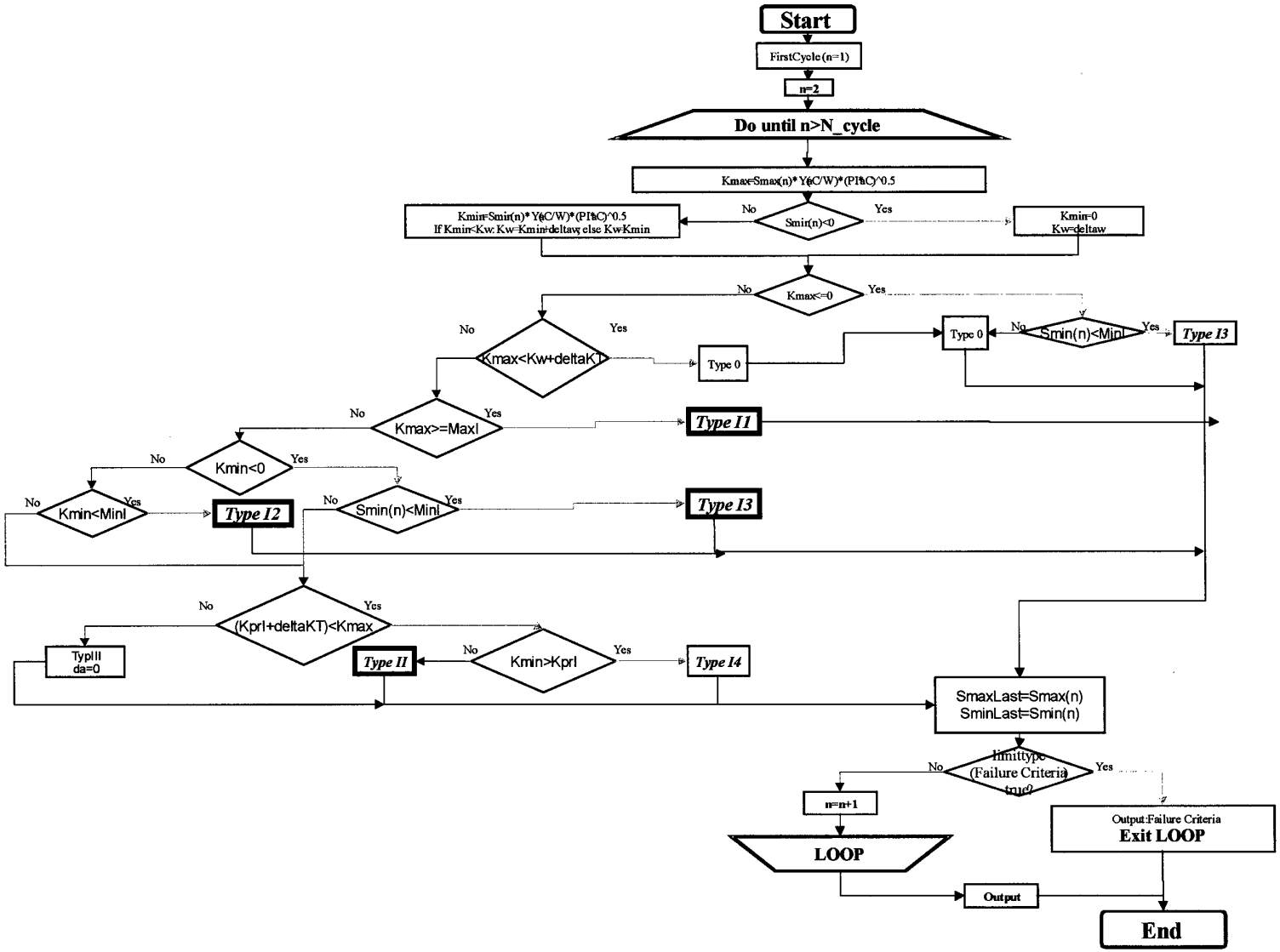
Start
FirstCycle(n=1)
n=2
Do until n>N_cycle
Kmax=Smax(n)*Y(C/W)*(PI%C)^0.5
Kmin=Smin(n)*Y(C/W)*(PI%C)^0.5
If Kmin<Kw; Kw=Kmin+deltaw; else Kw=Kmin
No
Smin(n)<0
Yes
Kmin=0
Kw=deltaw
No
Kmax<=0
Yes
No
Kmax<Kw+deltaKT
Yes
Type 0
Type 0
No
Smin(n)<MinI
Yes
Type I3
No
Kmax>=MaxI
Yes
Type I1
No
Kmin<0
Yes
No
Kmin<MinI
Yes
Type I2
No
Smin(n)<MinI
Yes
Type I3
No
(Kprl+deltaKT)<Kmax
Yes
TypIII
da=0
Type II
No
Kmin>Kprl
Yes
Type I4
SmaxLast=Smax(n)
SminLast=Smin(n)
No
limittype
(Failure Criteria)
true?
Yes
n=n+1
LOOP
Output:Failure Criteria
Exit LOOP
Output
End

Figure 6

2.2 Summary of material data required for operation of the K_{PR} model

Crack growth increments produced by individual load cycles are calculated from a plot of da/dN vs (K_{max}- K_{PR}), which is ΔK_{eff} reduced by ΔK_T. The reason for this somewhat unusual value on the x-axis is that ΔK_{eff} as defined in section 2.1 is zero for crack growth velocity below the threshold crack growth velocity (10^{-7} mm/cycle). (This is different to the definition by Elber where ΔK_T can larger than zero, yet the crack growth rate is below 10^{-7} mm/cycle since $\Delta K_{eff} \leq \Delta K_T$.) In the K_{PR} approach ΔK_{eff} would be zero, however zero can not be plotted in a logarithmic scale. This is the reason why the crack growth data are plotted versus K_{max}- K_{PR}. The software accounts for that and takes ΔK_T automatically into account. The function da/dN=f(ΔK_{eff}) must be established by experiment. ΔK_{eff} needs to be given in terms of K_{PR}, which can be done by applying the master curves in Figure 4 for constant amplitude loading (the lower line), in order to calculate an appropriate value for K_{PR} for the R ratio of interest, together with the equation

$$\Delta K_{eff} = K_{max} - K_{PR} - \Delta K_T$$

using a value for threshold ΔK_T obtained at very high R ratios using the K_{max} – constant testing procedure. The da/dN data used can be obtained by constant K_{max} growth rate data supplemented by high constant R values.

Once the relation between ΔK_{eff} and da/dN has been defined for constant amplitude loading, increments of growth produced by individual cycles in a variable amplitude cycle sequence can be calculated by establishing on a cycle by cycle basis, appropriate values of K_{max} and K_{PR} together with the intrinsic threshold ΔK_T to calculate appropriate growth increments. ΔK_T is a constant for a given material, and K_{max} in a load cycle is easy to establish. K_{PR} in a variable amplitude loading sequence will depend on a number of different factors. These are:

(a) The loading sequence itself

(b) Correction of loading conditions for crack closure effects. In many real cases this correction is negligible and can be eliminated (9, 10). If an error is made with this omission, it will always lead to conservative predictions.

(c) The equations of the master curves shown in Figure 4, which describe how K_{PR} changes with K_{max} and with UR for the extreme cases of a single overload and of multiple overload transitions.

(d) The function of K_{PR} describing its change between the single overload and the multiple overload master curves.

(e) The decline function of K_{PR}, describing how it will change as a function of crack growth increment – the Type II transition which is cycles dependent, – since the last type I load transition. The growth increment is expressed in terms of the progress through the fractional plastic zone size caused by the Type I transition.

(f) In addition to the requirements for constant amplitude crack growth data and the value of the basic threshold ΔK_T noted earlier, there is one further material parameter required, the yield stress σ_y. This is used in calculation of the crack tip plastic zone associated with the load excursion of the Type I transition.

Items c, d and e may all be determined by experiments of the type described earlier, and can be regarded as parameters exclusive to the material under consideration. Once these have been

defined, K_{PR} behaviour in the material may be deduced for all conditions of stress intensity range and mean, and for all loading sequences.

3. Material, test samples, loading spectra and experiment description

3.1 Materials

K_{PR} measurements were made on two type of materials, 7010-T76351 aluminium alloy and a quenched and tempered steel, SAE 4340. Specified composition of the materials is shown in Table 1 and the static mechanical properties are shown in Table 2.

Table 1
Specified composition of 7010 aluminium alloy

Element	Si	Fe	Cu	Mn	Mg	Cr	Zn	Zr	Al
Wt%	0.05	0.07	1.6	0.01	2.3	0.01	5.9	0.11	Balance

Table 2
Selected mechanical properties of 7010 T73651

Ultimate tensile strength (MPa)	0.2%proof strength (MPa)	% elongation	K_Q MPa $m^{1/2}$
518	456	14.7	33.5

Table 3

Specified composition of SAE 4360 Steel

Element	C	Mn	Si	Ni	Cr	Mo
Wt %	0.38-0.48	0.60-0.80	0.15-0.35	1.65-2.00	0.70-0.90	0.20-0.30

Table 4

Selected mechanical properties of SAE 4340, deduced from published data for properties of 4340 steel with a hardness 340 Brinell

Ultimate tensile strength (MPa)	0.2% Proof strength (MPa)	% Elongation	Fracture toughness (MPa $m^{1/2}$)
1100	1000	14	110

The steel will have a modulus of 207 GPa; the aluminium 70 GPa. The ductilities of the two materials are similar, but the steel has almost three times the toughness of the aluminium. This will influence greatly the form of the relation of growth rate da/dN with ΔK at high growth rates and also will change the effect of R ratio on growth rate in this regime. The proof strength of the aluminium is about half that of the steel, implying that the plastic zone size for any given load

transition will be about four times that of the steel. Stresses in the crack tip plastic zones will be correspondingly reduced in the aluminium alloy compared with those in the steel.

The 7010 material was supplied as 45 mm thickness plate, 610 mm x 610 mm. The 4340 steel was supplied as 100 mm diameter circular bar.

3.2 Test sample geometry

All tests were performed on Compact Tension (CT) samples with a thickness of 17.5 mm and a W dimension of 70 mm. A full drawing of the sample is shown in Figure 7.
In the case of the aluminium alloy plate, the compact tension samples were machined from the plate with the loading direction parallel to the rolling (L) direction in the plate, with crack growing in the transversee (T) direction, and the thickness of the CT sample in the ST direction. Two samples were taken from the thickness of the plate at each location. The surface of each sample was 2 mm from the top and bottom surface of the plate.

For the SAE 4340 CT samples, the loading direction was again parallel with the rolling direction of the bar, with the crack growing in the diametral direction. Two samples were taken side by side at each location along the bar.

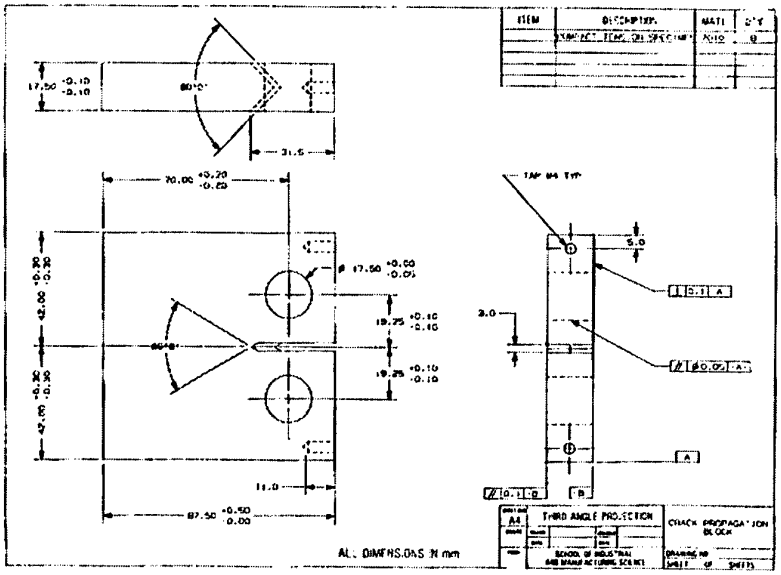

Figure 7 Dimensions of compact tension samples

3.3 Crack length measurement, fatigue test equipment and test description

Crack lengths in all tests were measured using a pulsed DC electrical potential technique. A pulsed constant current of 20 A was introduced into the specimen and the potential difference on each side of the sample notch was measured using a microvoltmeter. The potential output was related to crack length via an optical calibration made using a travelling microscope. The noise and drift in the system corresponded to a sensitivity of ± 0.05 mm and an absolute accuracy of ±0.1 mm. The relative accuracy is towards smaller values of about 20μm.

All tests were performed on a computer controlled servo hydraulic fatigue test machine of 50 kN capacity. Test frequencies were between 5 and 10 Hz. The following type of tests were performed.

(1) Constant load amplitude constant R ratio tests at R ratios of 0.1, 0.4, 0.7 and 0.9, as well as K_{max} constant tests at different maxima.

(2) Variable amplitude loading tests using defined spectra such as Falstaff, and Rotarix.

In test types 1 and 2, the loading parameters were held constant and the crack allowed to grow, the stress intensity values produced by the loads increasing with increasing crack length. In these tests, pairs of values of cycles and potential were recorded by a PC based system, and converted later into pairs of values of crack length and cycles and then into stress intensity and da/dN using procedures recommended in ASTM E647.

(3) Constant K_{max} decreasing ΔK tests

In these tests electrical potential data were converted into crack length during the test and used as input data to software controlling the test machine load so as to maintain constant K_{max} as the crack grew, but with ΔK decreasing by raising the K_{min}, to approach a threshold ΔK_T. The rate of approach to the threshold was consistent with the maximum rates of stress intensity reduction suggested in ASTM E647. A number of different samples were first precracked at constant amplitude, constant R of 0.1. The loading was then modified to set the desired K_{max} value, and then the crack was grown, maintaining the K_{max} value at that level, reducing the ΔK until a maximum growth rate of 10^{-7} mm/cycle was achieved. Different initial values of K_{max} were set in different samples.

(4) Automated tests to determine K_{PR} under a range of conditions

A suite of data processing and test machine control software was specially written to allow crack length data produced by the potential drop system to be used to follow the procedure for determination of K_{PR} described earlier in section 2. Identical test procedures were followed for 7010 aluminium and 4340 steel. Each compact tension sample was used for a number of determinations of K_{PR} under different conditions. Each measurement of K_{PR} was separated by 2-3 mm of crack growth under constant ΔK loading. Before the first measurement of K_{PR} in a sample, the crack was similarly grown for 2-3 mm. The tests performed under computer control were as follows:

(i) Determination of K_{PR} for constant amplitude loading

The fatigue cracks were first grown at a range of constant R and K_{max} values for 2-3 mm. For 7010 aluminium, the ΔK then was reduced to ΔK_B =1.5 MPa $m^{1/2}$. (ΔK_T = 1.2 MPa for 7010; for SAE 4340, ΔK_T = 2.5 MPa $m^{1/2}$, and ΔK_B was set =2.8 MPa $m^{1/2}$). 2 x10^5 cycles were applied at this level, and the crack length automatically monitored. If no growth was detected, K_{max} and K_{min} were both increased by δ= 0.2 MPa $m^{1/2}$ and 2 x 10^5 cycles applied again. The process was repeated until growth was detected during the 2 x 10^5 cycles. The resolution of the system of 0.1 mm implies the minimum growth rate detected was 0.1 / 2 x 10^5 = 5 x 10^{-7} mm/cycle. K_{PR} is then calculated from:

$$K_{PR} = \frac{K_{\max k} + K_{\max(k-1)}}{2} - \Delta K_T$$

Where $K_{max\ k}$ is the maximum stress intensity value at the level where crack growth was first detected, and $K_{max\ (k-1)}$ is the maximum stress intensity at the previous level.

(ii) Determination of K_{PR} after single overloads

A similar procedure was followed for the measurement of K_{PR} after overloads. After precracking at constant ΔK and R, an overload was applied to a stress intensity $K_{max\ OL}$, followed by a load reduction to K_{UL}. The K_{PR} measurement procedure was then followed as before. The overload and under loads applied were characterised in terms of the Over Load Ratio ($OLR= K_{max}/K_{maxOL}$) and Under load ratio ($U=K_{UL}/K_{max\ OL}$). K_{PR} was measured for a range of values of U and OLR. The parameters are illustrated schematically in Figure 8.

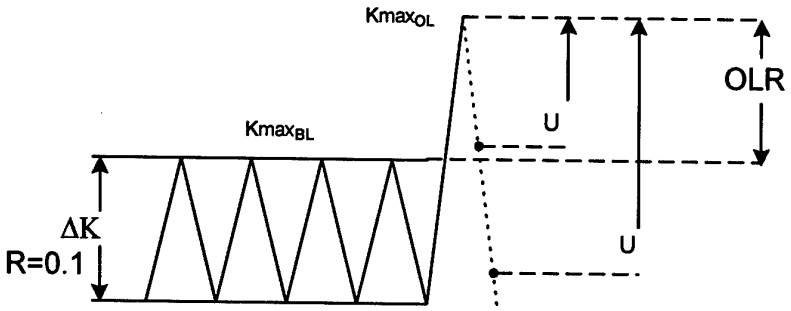

Figure 8 Schematic illustration of loading profile for K_{PR} determination after single overloads

(iii) Measurement of K_{PR} after multiple overloads

The procedure followed was identical to that described in (ii), but multiple overloads of 3, 5, 10, 50, and 100) were applied. The loading sequence is illustrated schematically in Figure 9.

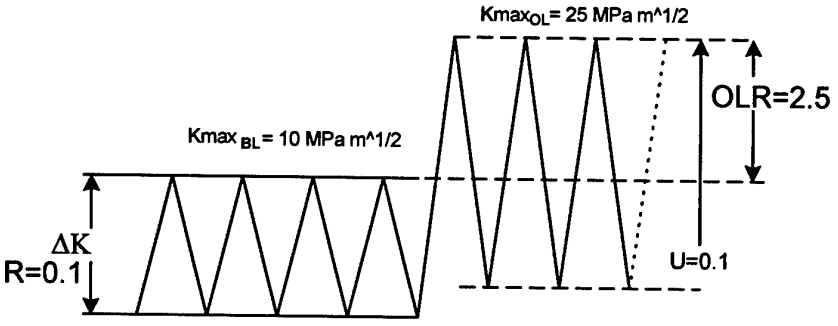

Figure 9 Schematic illustration of loading profile for K_{PR} measurement after multiple overloads

(iv) Measurement of decline of K_{PR} after an overload

The loading procedure for this is illustrated in Figure 10. A single overload of OLR 2.5 was applied followed by a return to the constant amplitude cycling. K_{PR} was measured at different distances from the overload application. Only a single measurement could be made after the application of an overload, so the entire process had to be repeated after each measurement, to obtain K_{PR} data at different crack growth increments after the overload application.

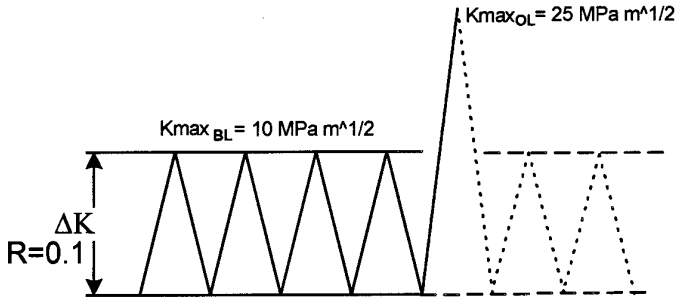

Figure 10 Schematic illustration of loading profile for measurement of K_{PR} decline

3.4 Measurements of closure

During all the above tests compact tension samples were fitted with a clip gauge mounted at the crack mouth to monitor the closure behaviour during the constant amplitude and overload testing. The closure data were used to calculate K_W, the effective minimum K in the loading cycle. This in turn was used to calculate R_{tip} the effective R ratio.

3.5 Loading spectra used in variable amplitude loading tests

The loading spectra used to validate the predictions of the K_{PR} model were Rotarix (1, 2, 3) and Falstaff (11). Three different variants of the Rotarix spectrum were used. Rotarix is a spectrum derived from strain measurements on the Westland Lynx rotorhead using the same sequence of manoeuvres as was used in the generation of the Helix and Felix (12) helicopter spectra. Helix and Felix were derived from strain measurements made on helicopter blades for hinged blades and fixed blades respectively. Identical procedures were used to derive the Rotarix spectrum, but substituting strain measurements made on the rotorhead, for the measurements made on the blades, in each of the manoeuvres in the sequence.

Like Helix and Felix, Rotarix represents a fixed sequence of 140 sorties or 190.5 hours of flight. As for Helix and Felix, turning points in the sequence are represented by levels, the levels being numbered from zero to 100 in intervals of 4. In its full form (Rotarix 16) the sequence consists of 1.98×10^6 cycles. 90% of these cycles are of range 16 or below, which originate in the rotor motion. There are 3 other variants of the spectrum in which cycles of progressively larger range have been removed. These are:

Rotarix 20, containing cycles of Range 20 and above, 1.13×10^5 cycles
Rotarix 24, containing cycles of Range 24 and above, 1.11×10^5 cycles
Rotarix 32, containing cycles of Range 32 and above, 5.14×10^4 cycles

The large numbers of small cycles in Rotarix 16 have R values of 0.7-0.9. These are interspersed with load excursions to lower loads caused by take off and landing cycles, together with other

manoeuvre loads. Thus Rotarix 16 is dominated by large numbers of high R cycles with underloads, whereas Rotarix 32 will be a spectrum consisting of larger lower R ratio cycles without underloads. A schematic of a section of Rotarix 16 is shown in Figure 11.

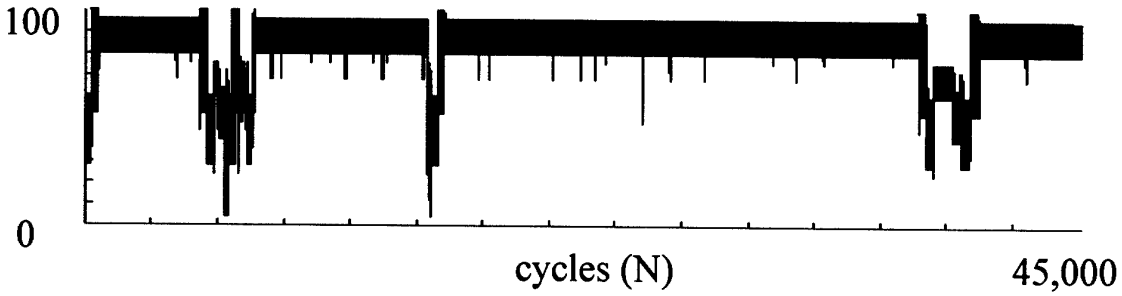

Figure 11 Load sequence from a short section of the original Rotarix load history

Falstaff (11) is a 32 level sequence of wing loads representing 200 flights of a military aircraft. It consists of 17988 cycles. These are of lower R than the cycles found in Rotarix.

For variable amplitude crack growth testing of both Falstaff and Rotarix, tension loads only were applied. In the case of Falstaff, this sequence contains a few excursions to small compression loads. To eliminate compression turning points, (and hence use CT samples for variable amplitude tests) the entire sequence was moved into tension, so that the minimum load was level zero instead of the usual spectrum where zero is level 7.5269.

To begin the variable amplitude tests, CT samples were precracked under constant amplitude loading, at R ratio of 0.1 and at peak loads which would give the desired K_{max} value for the variable amplitude test at the start crack length of 16-18 mm. This Kmax value was 10 MPa $m^{1/2}$ for the 7010 aluminium and 30 MPa $m^{1/2}$ for the SAE 4340 steel. These K_{max} values were chosen so that the level 16 cycles in Rotarix would be at or just over the threshold level for the material in question. Start K_{max} values for the Falstaff sequence were set equal to those used for Rotarix testing.

4. Results

4.1 K_{PR} measurements in 7010 aluminium

Table 5 shows the crack lengths and loading conditions for the constant amplitude measurements of K_{PR} in 7010 aluminium. Table 6 shows the values of K_{PR} which were measured for these conditions. The values changed with both K_{max} and R ratio, and were approximately between 40% at R values of 0.05-0.1 and 20% at R values of 0.7 of the nominal applied ΔK. Also shown in Table 6 are the values of the nominal R and modified R ratio, R_{tip}, the latter taking into account the closure experienced at the crack tip.

Table 5

Crack lengths, loading conditions for constant amplitude K_{PR} ; 7010 aluminium

Test		CAL01	CAL02	CAL03	CAL04	CAL05	CAL06	CAL07
$K_{max,i}$	$Mpam^{1/2}$	15	10	15	15	20	25	30
R		0.05	0.1	0.1	0.3	0.5	0.5	0.7
Initial crack length	M	0.015	0.019	0.022	0.0165	0.0212	0.019	0.029
Crack lgth. Increment	M	0.002	0.0024	0.003	0.0025	0.0023	0.002	0.001
Crack growth rate	m/cycle	$2.4\ 10^{-7}$	$9\ 10^{-8}$	$3.2\ 10^{-7}$	$2\ 10^{-7}$	$2.8\ 10^{-7}$	$5.5\ 10^{-7}$	$5.1\ 10^{-7}$

Table 6

K_{PR} values for constant amplitude loading; 7010 aluminium

Test	$K_{max,i}$ (Mpa $m^{1/2}$)	R	Crack length (m)	UR(R_{tip})	K_{PR} (MPa $m^{1/2}$)	$K_{max,k}$ (MPa $m^{1/2}$)	$K_{max,k-1}$ (MPa $m^{1/2}$)
CAL01	15	0.05	0.017	0.08	6.3	7.6	7.4
CAL02	10	0.1	0.024	0.13	4.3	5.6	5.4
CAL03	15	0.1	0.025	0.12	6.4	7.7	7.5
CAL04	15	0.3	0.019	0.3	8.2	9.5	9.3
CAL05	20	0.5	0.025	0.5	12.7	14	13.8
CAL06	25	0.5	0.021	0.5	16.5	17.8	17.6
CAL07	30	0.7	0.03	0.7	22.9	24.2	24

Table 7 shows the loading conditions and crack lengths for K_{PR} measurements after a single overload, unloading after the overload to a series of different values. Table 8 gives values for the overload and underload ratios and the measured value of K_{PR}. Values of K_{PR} generally follow the same trends with increasing values of U the underload ratio, as for constant amplitude loading with increasing R.

If both constant amplitude and single overload values of K_{PR} are normalised with respect to K_{max} (or $K_{max\ OL}$ in the case of the single overloads), and plotted against R_{tip} or more generally UR, the two sets of points form two curves, as shown in Figure 12 The best fit polynomial curves through these points have the expressions:

For constant amplitude loading

$$K_{PR}/K_{max} = 0.383 + 0.400UR + 0.248(UR)^2 - 0.0335(UR)^3$$

For single overloads

$$K_{PR} / K_{\max OL} = 0.294 + 0.394(UR) + 0.419(UR)^2 - 0.1085(UR)^3$$

The two curves are relatively close to each other with the single overload curve falling below the constant amplitude one (but corresponding to the higher respective maximum load).

Table 7

Crack length, loading data for K_{PR} after single overloads; 7010

Test		OLR01	OLR02	OLR03	OLR04	OLR05	OLR06
$K_{max,i}$	MPa $m^{1/2}$	10	10	10	10	10	10
R		0.1	0.1	0.1	0.1	0.1	0.1
Init crack length	m	0.034	0.02	0.04	0.0366	0.023	0.0267
Crck lngth increment	m	0.002	0.002	0.002	0.0024	0.002	0.002
Crack growth rate	m/cycle	$8\ 10^{-8}$	10^{-7}	10^{-7}	$9\ 10^{-8}$	10^{-7}	$9\ 10^{-8}$

Table 8

K_{PR} data for single overloads; 7010 aluminium

	$K_{max,BL}$ MPa $m^{1/2}$	R	$K_{max,OL}$ MPa $m^{1/2}$	OLR	Crack length (m)	U	$UR(R_{tip})$	K_{PR} MPa $m^{1/2}$	$K_{max,k}$ MPa $m^{1/2}$	$K_{max,k-1}$ MPa $m^{1/2}$
OLR01	10	0.1	20	2	0.036	0.1	0.26	8	9.3	9.1
OLR02	10	0.1	20	2	0.022	0.3	0.3	9.2	10.5	10.3
OLR03	10	0.1	20	2	0.0432	0.5	0.5	12.2	13.5	13.3
OLR04	10	0.1	20	2	0.039	0.7	0.7	14.6	15.9	15.7
OLR05	10	0.1	25	2.5	0.025	0.1	0.12	9.5	10.8	10.6
OLR06	10	0.1	25	2.5	0.0287	0.5	0.5	14.4	15.7	15.5

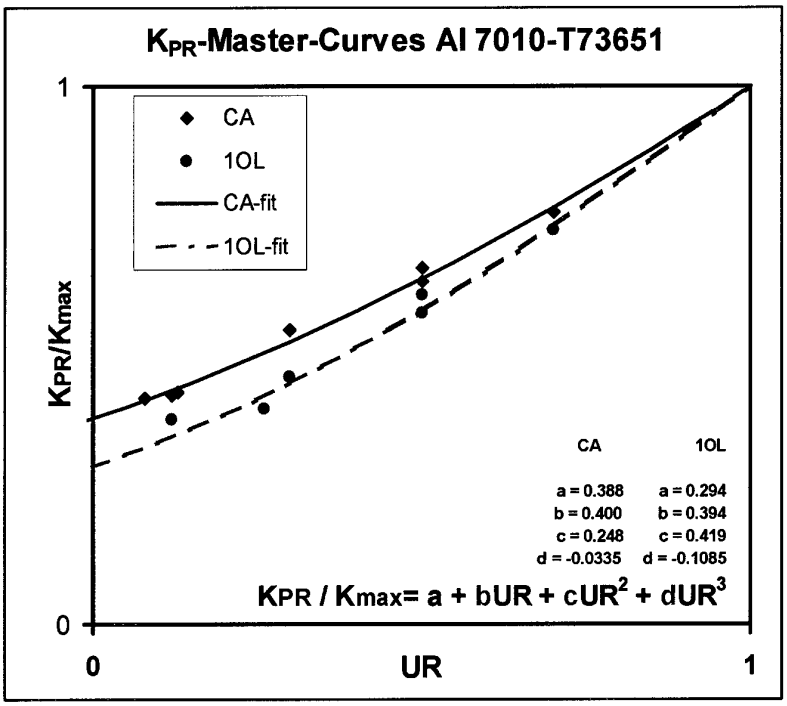

Figure 12 Master curves for 7010 aluminium; constant amplitude and single overload loading

Table 9 shows crack length and loading conditions for the experiments to determine the influence of multiple overloads on K_{PR}. K_{max} was set at 10 for all these experiments with an R value of 0.1. Multiple overloads of 3, 5, 10, 50 and 100 were applied. Table 10 shows that values of K_{PR} increase with increasing numbers of overloads, gradually moving back to the new constant amplitude loading. Figure 13 shows a plot of K_{PR} vs number of repeated overloads for 7010 aluminium.

Table 9
Crack length and loading conditions for multiple overload tests; 7010

Test		MOL01	MOL02	MOL03	MOL04	MOL05	MOL06
$K_{max,i}$	MPa $m^{1/2}$	10	10	10	10	10	10
R		0.1	0.1	0.1	0.1	0.1	0.1
Initial crack lngth	m	0.023	0.03	0.0334	0.0359	0.0164	0.014
Crack length increment	m	0.002	0.0028	0.002	0.002	0.002	0.0016
Crack growth rate	m/cycle	$8\ 10^{-8}$	10^{-7}	10^{-7}	$9\ 10^{-8}$	10^{-7}	$9\ 10^{-8}$

Table 10

K_{PR} values after multiple overloads; 7010 aluminium

	$K_{max,BL}$ (MPa $m^{1/2}$)	R	OLR	Crack length (m)	$K_{PR,OL}$ (MPa $m^{1/2}$)	$K_{max,k}$ (MPa $m^{1/2}$)	$K_{max,k-1}$ (MPa $m^{1/2}$)	Number of over loads
MOL01	10	0.1	2.5	0.025	9.5	10.8	10.6	1
MOL02	10	0.1	2.5	0.0323	9.4	10.7	10.5	3
MOL03	10	0.1	2.5	0.0354	9.6	10.9	10.7	5
MOL04	10	0.1	2.5	0.0379	9.6	10.9	10.7	10
MOL05	10	0.1	2.5	0.0184	10.4	11.7	11.5	57
MOL06	10	0.1	2.5	0.0156	11	12.3	12.1	100

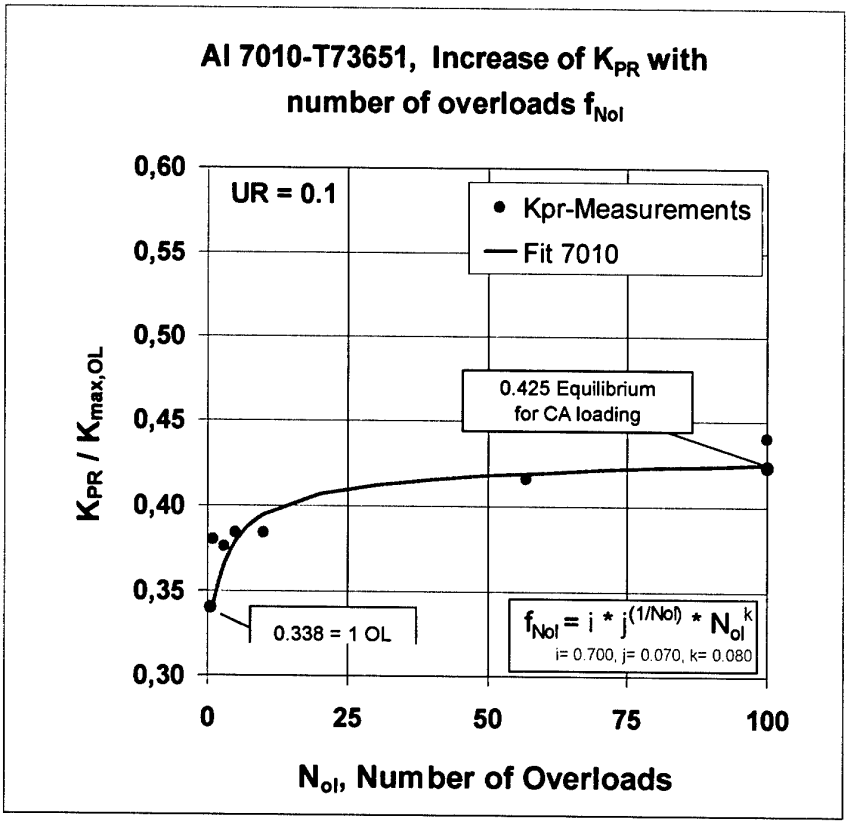

Figure 13 Effect of multiple overloads on K_{PR}; 7010 aluminium alloy

Finally, Table 11 shows the crack lengths and loading conditions for the tests to measure K_{PR} decline after the application of an overload. K_{max} was 10 MPa $m^{1/2}$ and R was 0.1 for all these tests. The overload ratio was 2.5. K_{PR} declined from 8.3 to 7.3 MPa $m^{1/2}$ over a growth increment of about 80% of the calculated plastic zone size. The data are shown in Table 12. Figure 14 represents this trend graphically.

Table 11 : Crack lengths and loading data for K_{PR} decline; 7010 aluminium

Test		dec01	dec02	dec03	dec04
$K_{max,i}$	MPa $m^{1/2}$	10	10	10	10
R		0.1	0.1	0.1	0.1
Initial crack length	M	0.018	0.0238	0.02	0.0266
Crack length increment	M	0.002	0.002	0.002	0.0026
Crack growth rate	m/cycle	$8\ 10^{-8}$	10^{-7}	10^{-7}	$9\ 10^{-8}$

Table 12

K_{PR} decline data; 7010 aluminium alloy

	$K_{max,BL}$ (MPa $m^{1/2}$)	R	OLR	Crack length (m)	$K_{PR,OL}$ (MPa $m^{1/2}$)	$K_{max,k}$ (MPa $m^{1/2}$)	$K_{max,k-1}$ (MPa $m^{1/2}$)	dist into plastic zone (%)	N_{after}
Dec01	10	0.1	2.5	0.020	8.3	9.6	9.4	0.05	100
Dec02	10	0.1	2.5	0.0258	8.6	9.9	9.7	0.15	800
Dec03	10	0.1	2.5	0.022	7.6	8.9	8.7	0.4	1600
Dec04	10	0.1	2.5	0.029	7.3	8.6	8.4	0.8	3000

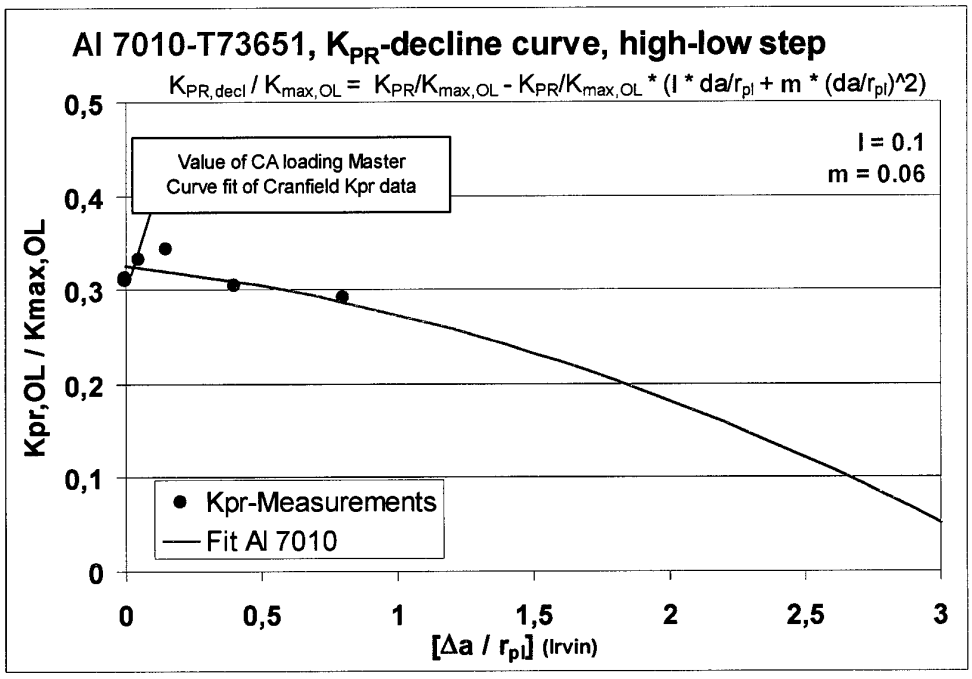

Figure 14 K_{PR} decline data for 7010 aluminium, plotted against crack growth through the plastic zone

4.2 K_{PR} measurements in SAE 4340 steel

Table 13 shows the crack length and loading conditions for the tests to determine K_{PR} under constant amplitude loading for SAE 4340 steel. As for the aluminium alloy, R values were between 0.05 and 0.7. Table 14 shows the values of K_{PR} obtained. As expected they were significantly greater than those for aluminium. They were also a significantly greater fraction of both the ΔK and the K_{max} level of the load cycle. As figure 15 shows, K_{PR}/K_{max} for 4340 steel was between 10-25% greater than for 7010 aluminium alloy at a given value of UR. Otherwise the forms of the curves were similar to those of the aluminium.

Table 13

Crack lengths and loading conditions for constant amplitude K_{PR}; 4340 steel

Test	Units	CAL01	CAL02	CAL03	CAL04	CAL05	CAL06	CAL07
$K_{max,i}$	MPa $m^{1/2}$	20	20	25	25	30	35	40
R		0.05	0.1	0.1	0.3	0.5	0.5	0.7
Initial crack length	M	0.015	0.0169	0.0188	0.0208	0.0278	0.0258	0.0295
Crack increment	M	0.0015	0.0024	0.0014	0.0034	0.0015	0.0016	0.0015
Crack growth rate	m/cycle	$4\ 10^{-8}$	$4.3\ 10^{-8}$	$7.2\ 10^{-8}$	$4.5\ 10^{-8}$	$3.3\ 10^{-8}$	$3.7\ 10^{-8}$	$1.8\ 10^{-8}$

Table 14: K_{PR} data for single overloads 4340 steel

Test	$K_{max,i}$ MPa $m^{1/2}$	R	Crack length (m)	UR (R_{tip})	K_{PR} MPa $m^{1/2}$	$K_{max,k}$ MPa $m^{1/2}$	$K_{max,k-1}$ MPa $m^{1/2}$
CAL01	20	0.05	0.0165	0.09	11.3	13.9	13.7
CAL02	20	0.1	0.0183	0.11	11.4	14	13.8
CAL03	25	0.1	0.0202	0.11	13.9	16.5	16.3
CAL04	25	0.3	0.0242	0.3	15.4	18	17.8
CAL05	30	0.5	0.0293	0.5	20.5	23.1	22.9
CAL06	35	0.5	0.0274	0.5	23.9	26.5	26.3
CAL07	40	0.7	0.031	0.7	31.7	34.3	34.1

Tables 15 and 16 show the crack length and loading conditions and the resultant K_{PR} values for 4340 steel subjected to single overloads. Overload and underload ratios were identical to those used for the 7010 aluminium alloy. The values of K_{PR} expressed as a fraction of $K_{max\ OL}$ after single overloads show again a reduction when compared with the constant amplitude data. The values obtained are once again between 10 and 25% greater than the ones obtained in 7010 aluminium. Plots of K_{PR}/K_{max} vs UR for SAE 4340 are shown in Figure 15 for both constant amplitude and single overload data. The form of the curves is similar to the 7010 aluminium.

For constant amplitude loading the change of K_{PR}/K_{max} with UR can be expressed as:

$$K_{PR}/K_{\max} = 0.57 + 0.14(UR) + 0.20(UR)^2 + 0.09(UR)^3$$

For single overload s the expression is:

$$K_{PR}/K_{\max OL} = 0.4 + 0.32(UR) + 0.24(UR)^2 + 0.04(UR)^3$$

Table 15

Crack length and loading conditions K_{PR} single overloads 4340 steel

Test		OLR01	OLR02	OLR03	OLR04	OLR05	OLR06
$K_{max,i}$	MPa $m^{1/2}$	20	20	20	20	20	20
R		0.1	0.1	0.1	0.1	0.1	0.1
Initial crack length	m	0.0146	0.0164	0.0181	0.0199	0.0326	0.0218
Crack length increment	m	0.0015	0.0013	0.0013	0.0013	0.0015	0.001
Crack growth rate	m/cycle	$3.4\ 10^{-8}$	$3.8\ 10^{-8}$	$3.7\ 10^{-8}$	$3.8\ 10^{-8}$	$3.5\ 10^{-8}$	$3.4\ 10^{-8}$

Table16

K_{PR} data for single overloads, 4340 steel

	$K_{max,BL}$ $MPm^{1/2}$		$K_{max,OL}$ MPa $m^{1/2}$	OLR	Crack length (m)	U	UR (R_{tip})	K_{PR} MPa $m^{1/2}$	$K_{max,k}$ MPa $m^{1/2}$	$K_{max,k-1}$ MPa $m^{1/2}$
OLR01	20	0.1	40	2	0.0161	0.1	0.13	17.3	19.9	19.7
OLR02	20	0.1	40	2	0.0177	0.3	0.3	20.1	22.7	22.5
OLR03	20	0.1	40	2	0.0194	0.5	0.5	24.6	27.2	27
OLR04	20	0.1	40	2	0.0212	0.7	0.7	30.2	32.8	32.6
OLR05	20	0.1	50	2.5	0.0341	0.1	0.104	21.3	23.9	23.7
OLR06	20	0.1	50	2.5	0.0231	0.5	0.5	31.1	33.7	33.5

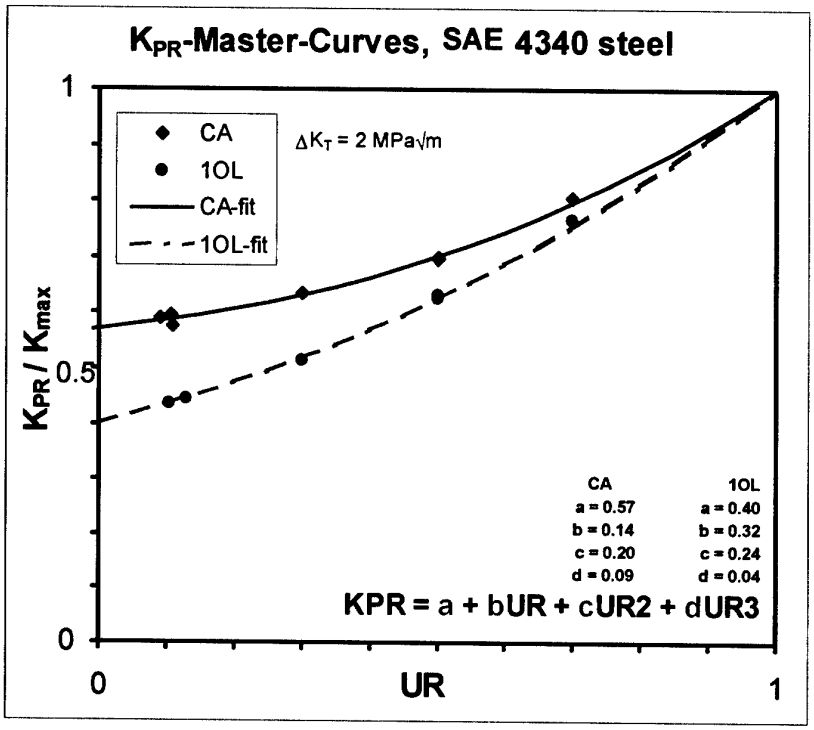

Figure 15 K_{PR} master curves for constant amplitude and single overloads; 4340 steel

Table 17

Loading conditions and crack lengths for multiple overloads 4340 steel

Test		MOL01	MOL02	MOL03	MOL04	MOL05	MOL06
$K_{max,i}$	MPa $m^{1/2}$	20	20	20	20	20	20
R		0.1	0.1	0.1	0.1	0.1	0.1
Initial crack length	m	0.0326	0.0238	0.0252	0.0277	0.0306	0.0325
Crack length increment	m	0.0015	0.0012	0.0011	0.0012	0.0008	0.0012
Crack growth rate	m/cycle	$3.5\ 10^{-8}$	$3.5\ 10^{-8}$	$3.6\ 10^{-8}$	$2.5\ 10^{-8}$	$3.5\ 10^{-8}$	$2.9\ 10^{-8}$

Table 18

K_{PR} values for multiple overloads 4340 Steel

	$K_{max,BL}$ (MPa $m^{1/2}$)	R	OLR	Crack length (m)	$K_{PR,OL}$ (MPam$^{1/2}$)	$K_{max,k}$ (MPam$^{1/2}$)	$K_{max,k-1}$ (MPam$^{1/2}$)	No. of Overl.
MOL01	20	0.1	2.5	0.0341	21.3	23.9	23.7	1
MOL02	20	0.1	2.5	0.02	22.6	25.2	25	3
MOL03	20	0.1	2.5	0.0263	25	27.6	27.4	5
MOL04	20	0.1	2.5	0.0299	26.1	28.7	28.5	10
MOL05	20	0.1	2.5	0.0314	26.8	29.4	29.2	50
MOL06	20	0.1	2.5	0.0337	27.4	30	29.8	100

Tables 17 and 18 show the loading conditions and the test results for the application of multiple overloads to the SAE 4340 steel. The K_{PR} values show a similar trend to the 7010 alloy with rapidly increasing values of K_{PR} at first and an asymptotic approach to the value determined previously for the constant amplitude loading case. The data are represented graphically in Figure 16.

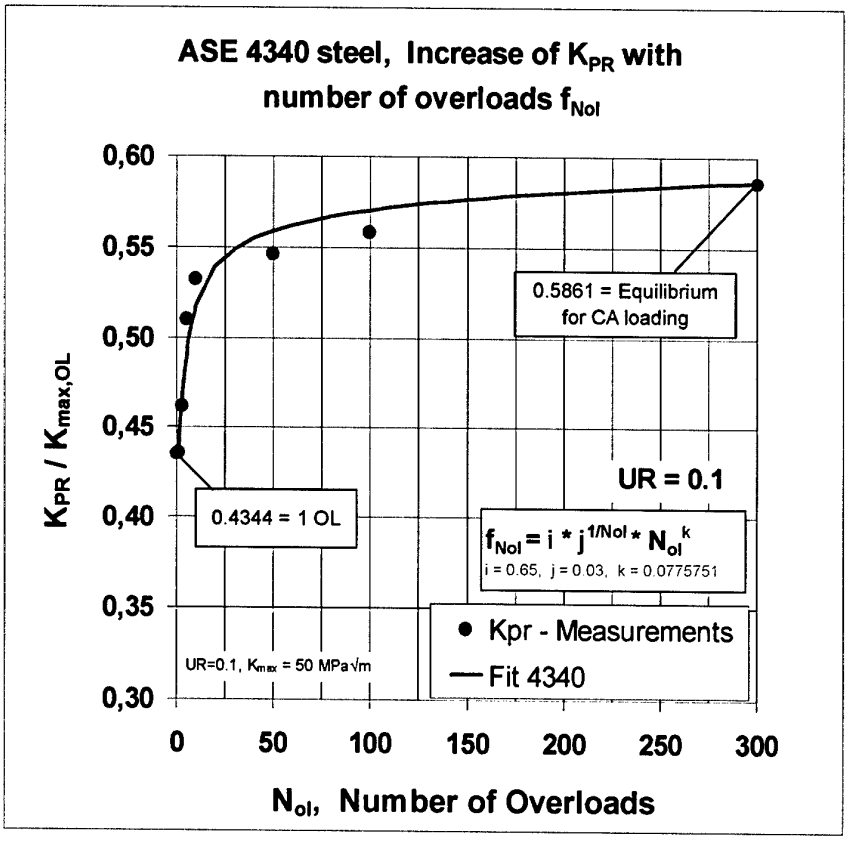

Figure 16 K_{PR} changes with multiple overloads; 4340 steel

Tables 19 and 20 show the loading and crack length data and the test results for the K_{PR} decline curve for the 4340 steel. The behaviour is similar to that of the 7010 aluminium. The decline behaviour is plotted against the crack incremental growth represented as a fraction of the plastic zone size in Figure 17.

Table 19
Loading and crack length data for K_{PR} decline curve; 4340 steel

Test		dec01	dec02	dec03	dec04
$K_{max,i}$	MPa $m^{1/2}$	30	30	30	30
R		0.1	0.1	0.1	0.1
Init crack length	m	0.0147	0.039	0.0365	0.034
Crack length increment	m	0.0009	0.0038	0.0013	0.0015
Crack growth rate	m/cycle	10^{-7}	$1.1\ 10^{-7}$	$1.1\ 10^{-7}$	$9.6\ 10^{-8}$

Table 20
K_{PR} data for decline behaviour; 4340 steel

	$K_{max,BL}$ MPam$^{1/2}$	R	OLR	Crack length (m)	$K_{PR,OL}$ MPam$^{1/2}$	$K_{max,k}$ MPam$^{1/2}$	$K_{max,k-1}$ MPam$^{1/2}$	Penetr. in plastic zone %	N_{after}
Dec01	30	.0.1	1.67	0.0166	21.85	24.45	24.25	5	350
Dec02	30	00.1	1.67	0.0428	21.35	23.95	23.75	15	1050
Dec03	30	00.1	1.67	0.0378	17.4	20	19.8	40	2800
Dec04	30	00.1	1.67	0.0355	17	19.6	19.4	80	5600

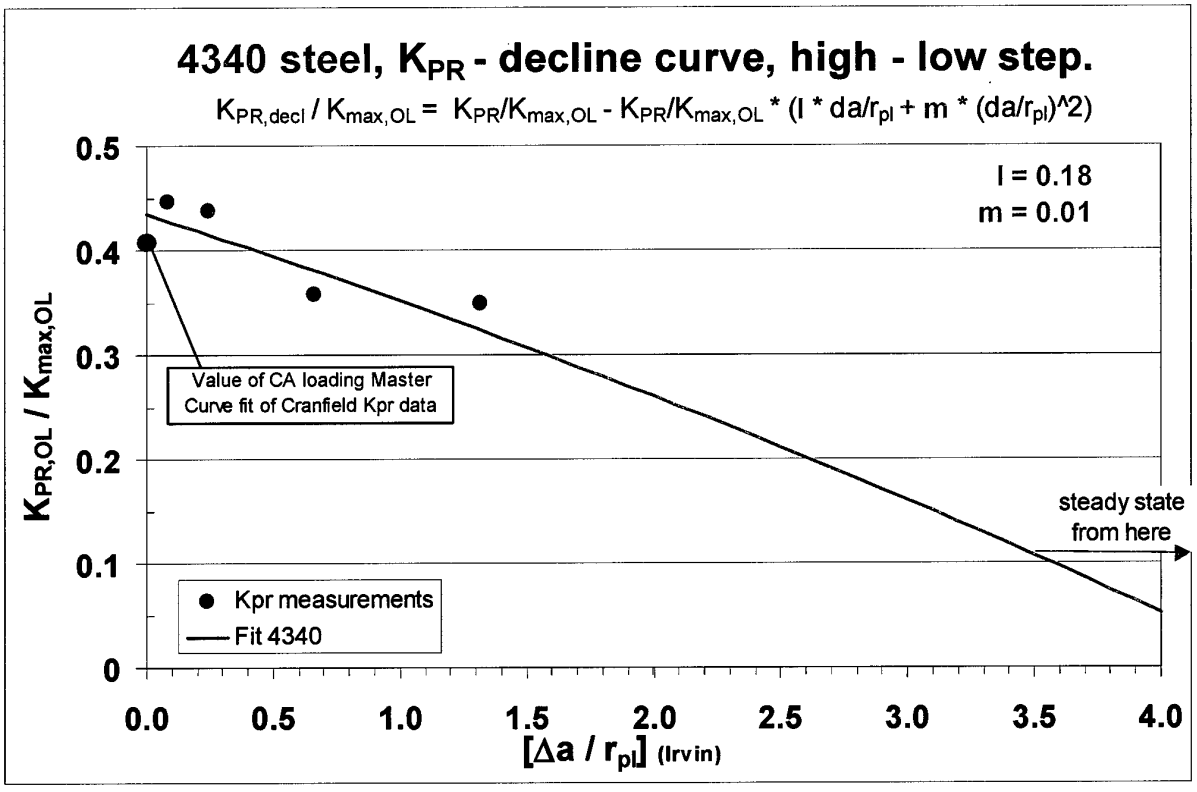

Figure 17 K_{PR} decline behaviour, 4340 steel

An example for a late recovery is indicated in Figure 17. The average distance for the re-establishment of a steady state K_{PR} level is however about two plastic zone sizes.

4.3 Crack growth data -both materials

To calculate a cycle by cycle crack growth increment, crack growth data are needed as well as K_{PR} data. Figure 18 shows da/dN data for 7010 aluminium at constant R ratio. together with data from data tables for this alloy. For both materials, the Forman fit data and the tabular input data are indicated in the figures. These data are not needed for the K_{PR} model, but for the other models that are also evaluated in this project. The data show significant R ratio effects, which are most marked at the low growth rate near threshold region and at the high ΔK fast growth rate region.

Figure 19 shows da/dN vs. ΔK data for constant K_{max} tests for starting K_{max} values of 12, 18, 24, and 30 MPa $m^{1/2}$. Starting R ratios were as low as 0.17, finishing R ratios at threshold were 0.8-0.9. There is a notable absence of any effect of crack closure in these data. The value of ΔK_T obtained in these tests, 1.3 MPa $m^{1/2}$, was identical to that found in the constant R testing for R ratio of 0.75 and above. This was the value used as the basis for the ΔK range used in the K_{PR} test measurements.

Both R constant and K_{max} constant test data were used in the derivation of the growth rate master curve- a plot of da/dN vs ΔK_{eff} with ΔK_{eff} defined as K_{max}-K_{PR}-ΔK_T. A plot of da/dN vs (K_{max} - K_{PR}) is shown in Figure 20 for 7010 aluminium. The term ΔK_T has been omitted as it would result in a zero value for ΔK_{eff} at the threshold and cause plotting problems on a log scale. The intrinsic threshold value for Al 7010 – T73651 is ΔK_T = 1.3 MPa $m^{1/2}$. The master curve for constant amplitude loading collapses the data very well. The data are fed into the software as a tabular input with about 100 data points for a good fit.

All K_{max} constant data and the constant R data for 0.75 and above are accommodated within the scatter band in Figure 20. A good correlation is obtained. The effective crack growth curves that are used for the K_{PR} model are shown as a red line. The lower R constant tests data are not included since they would have to be corrected for microstructurally induced closure which was done in (4). Equivalent data for SAE 4340 steel is shown in Figures 21, 22 and 23. These show the constant R ratio growth rate data, constant K_{max} growth rate data and the plot of (K_{max} – K_{PR}) vs da/dN. The data are less extensive than is available for the 7010 aluminium alloy, and it can be seen in Figure 23 that the compression of the data in the plot of da/dN vs (K_{max}-K_{PR}) is less successful than for 7010 as there is some residual scatter. The tabular input for 4340 had to be extrapolated and adjusted since the crack growth rates at R = 0.1 were in a certain region of ΔK higher than those of R = 0.3 which is physically impossible, indicating testing problems.

4.4 Variable amplitude validation testing

After precracking of the compact tension samples, crack growth tests under variable amplitude loading were performed on both 7010 and 4340 materials. Tests were performed under the Rotarix 16, 20, and 32 and under the Falstaff loading histories. The crack length vs cycles data obtained were compared with those calculated using the K_{PR} approach. In all cases, the predictions were made before the experimental data were known. In addition, comparison was made with the predictions made using the AFGROW based Closure, Willenborg and Willenborg models, and also the FASTRAN model. The results are presented in section 5.

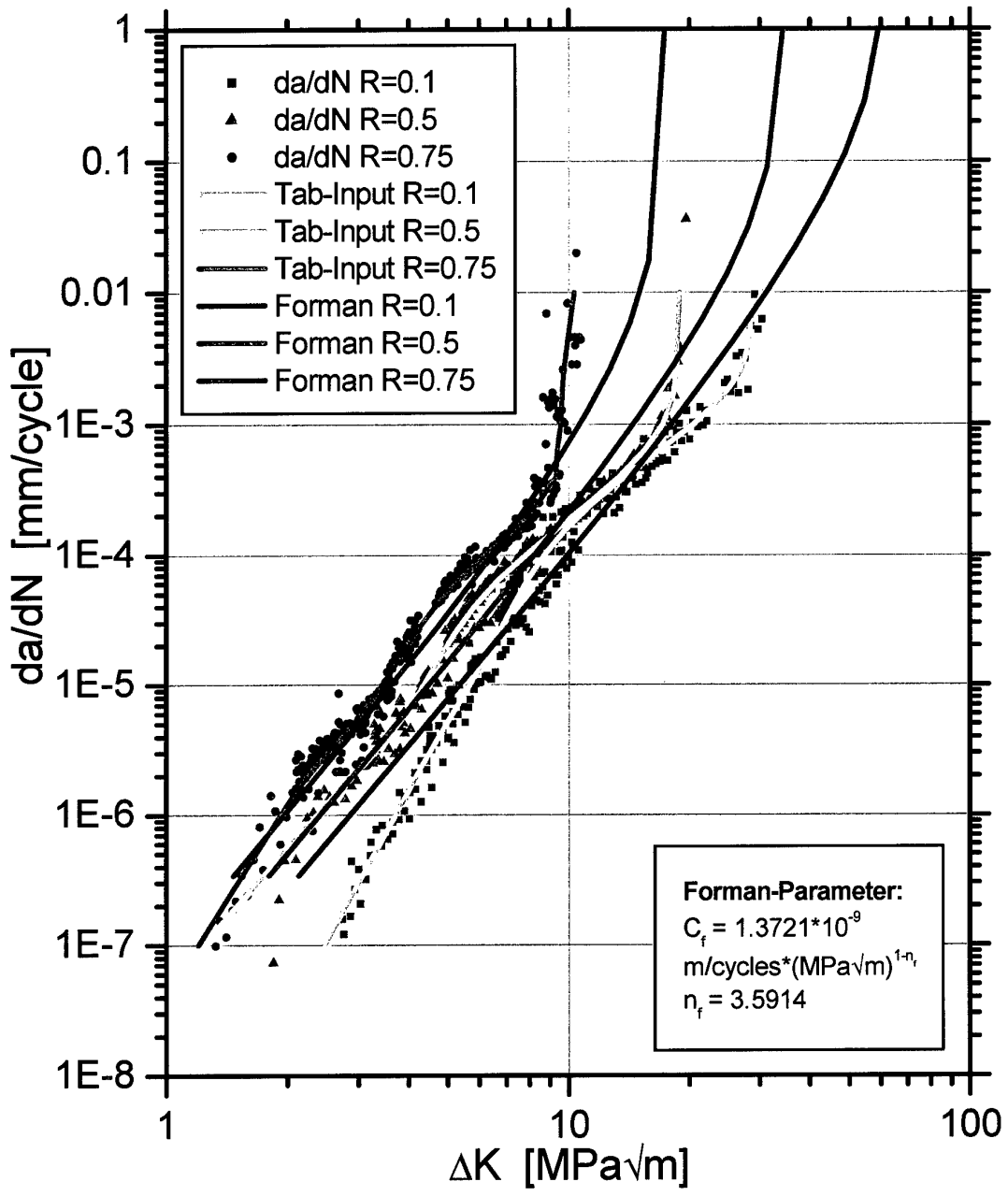

Figure 18 da/dN vs ΔK constant R ratio tests 7010 aluminium

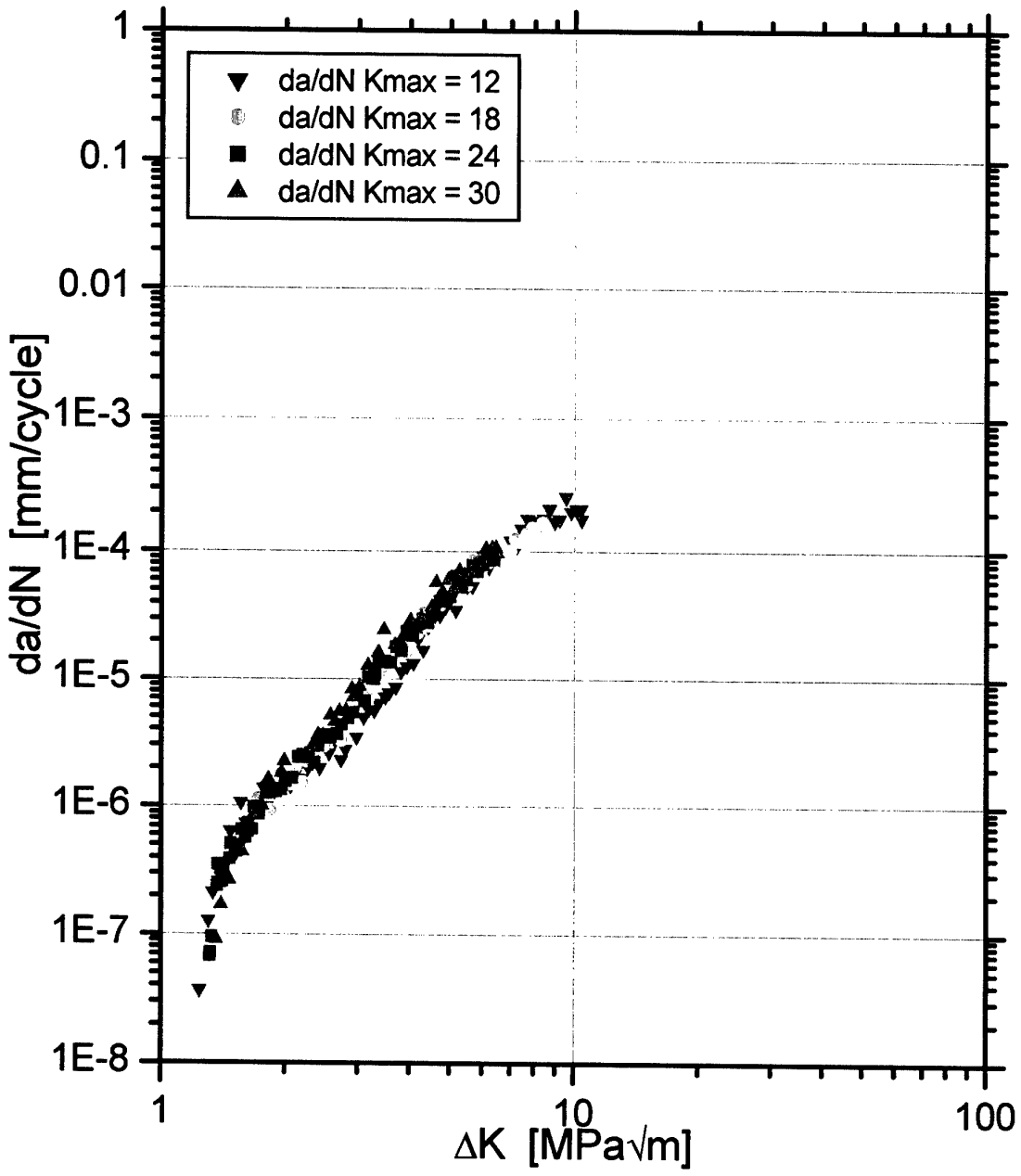

Figure 19 da/dN vs ΔK constant K_{max} tests, 7010 aluminium

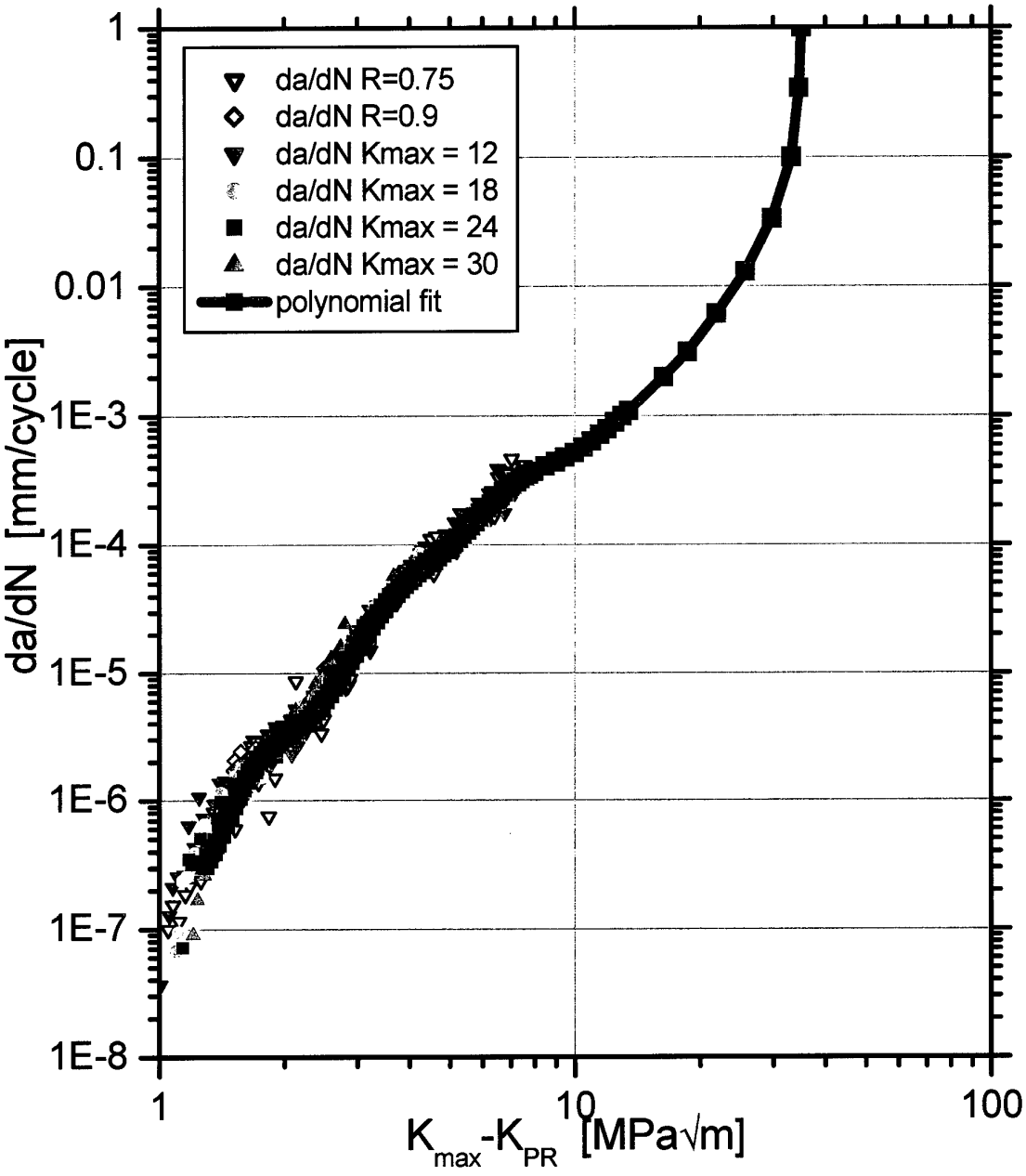

Figure 20 da/dN vs. K_{max}-K_{PR} 7010 aluminium alloy

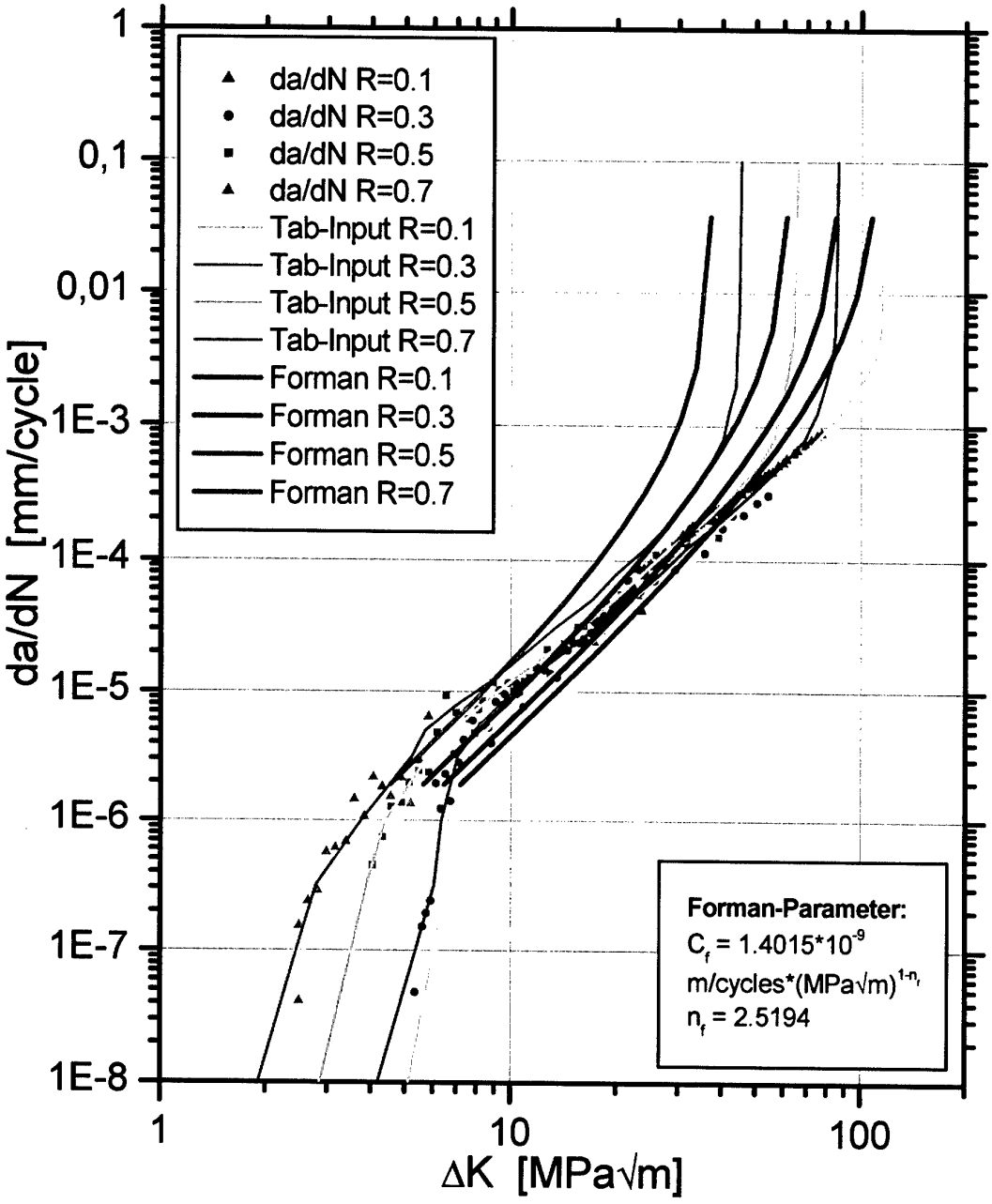

Figure 21 da/dN vs ΔK constant R tests for 4340 steel

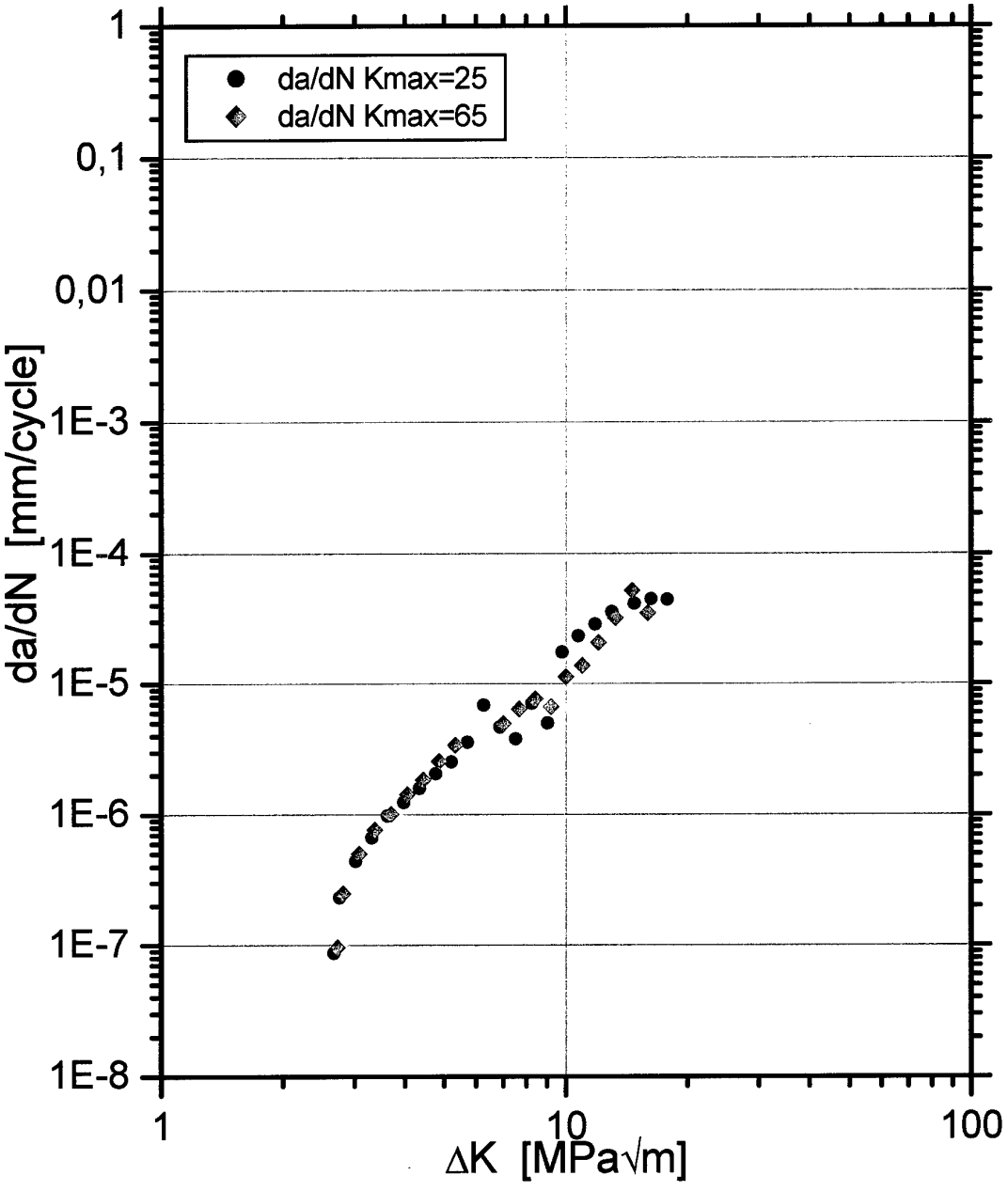

Figure 22 da/dN vs ΔK; constant K_{max} tests, 4340 steel

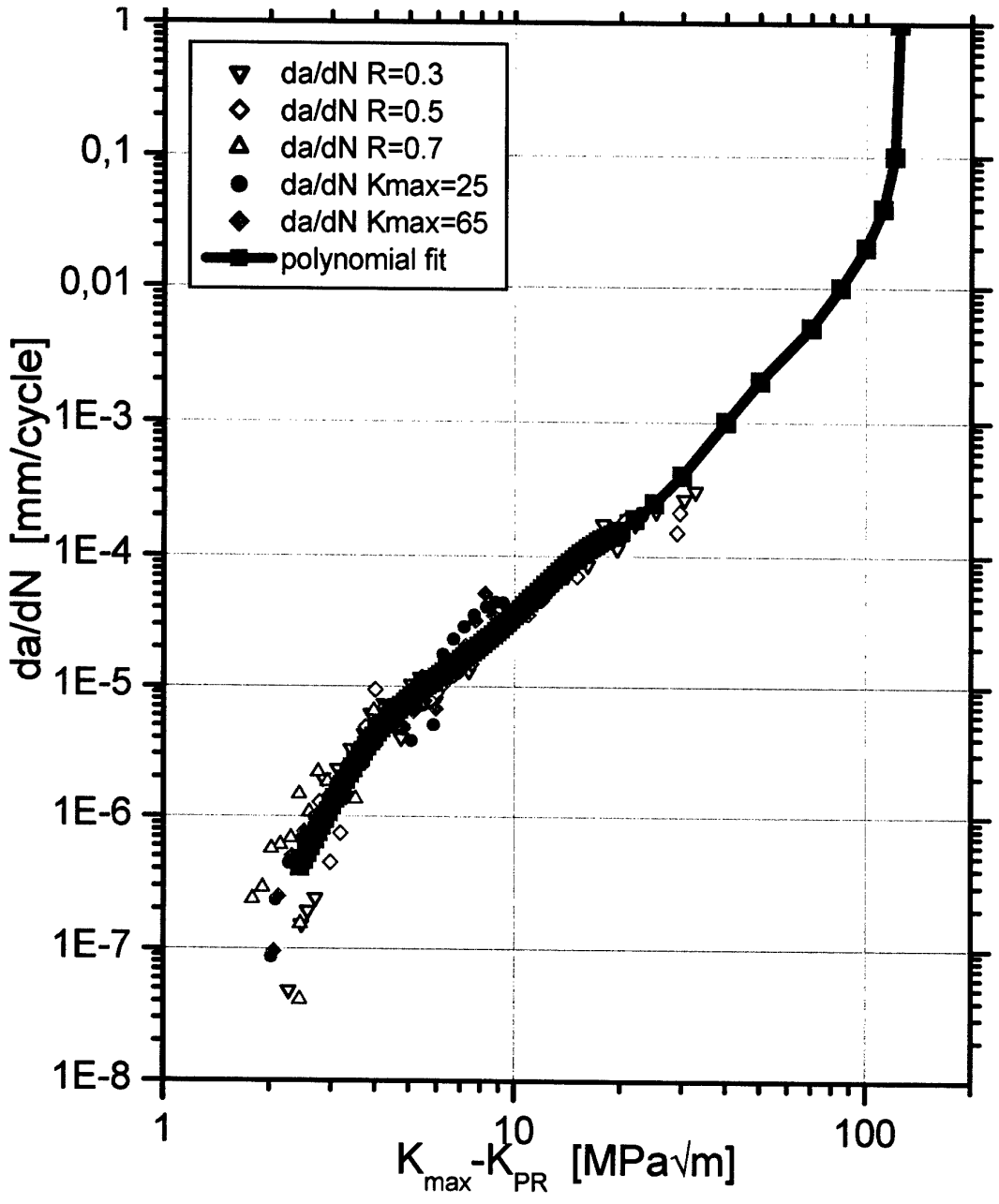

Figure 23 da/dN vs (K_{max}-K_{PR}) master curve for 4340 steel

5 Analysis

5.1 Example Calculations with Block Loading Sequences

As a first investigation of the K_{PR} model, the trace of K_{PR} under variable amplitude loading for simple loading sequences was analyzed. The K_{PR} values under block loading sequences were calculated and the resulting cycle by cycle K_{PR} values were put into an output file. The results can be seen in Figures 24-32.

The case of a single overload is shown in Figure 24. K_{PR} increases immediately after an overload and then declines due to the crack growth dependent transition. All small loading cycles are Type II cycles. K_{PR} does not decline very far, since the next overload follows after 1000 cycles.

The case where K_{PR} declines to a steady state value after an overload is shown in Figure 25. The retarding effect lasts here for about 1100 cycles. The case where the overload is succeeded by an unloading cycle which lowers K_{PR} is shown in Figure 26. The steady state K_{PR} value is lowered by about 2 MPa $m^{1/2}$ despite the prior overload. The current K_{PR} value is now below the steady state K_{PR} for constant amplitude loading. This case is modeled such that K_{PR} is linearly increased to reach the steady state K_{PR} value at the end of the plastic zone created by the last Type I cycle (the overload). In cases of highly variable loading where amplitude and R value of the following the Type II cycles change, the same procedure is done for every respective Type II cycle. The opposite case where the underload is first and then the overload is applied is shown in Figure 27. K_{PR} is first significantly lowered by the underload. The succeeding overload is thus producing a relatively large crack growth increment. The overload itself however increases K_{PR} again and then a decline follows as usual. These two last examples clearly demonstrate the ability of the model to account for load sequence effects. Whether it does it quantitatively correctly is to be determined later in the program.

Figure 28 and Figure 29 show that different block sizes in the same block loading sequence lead to a different picture in the level of K_{PR}. The case for a higher difference in the R values of the respective loading blocks is shown in Figure 30 and Figure 31. In Figure 30 the difference in the R values allows K_{PR} to reestablish the steady state value, whereas the drop to a lower loading sequence in Figure 31 leads to a decline that is followed by the next high block before the steady state value is established.

In the spectrum in Figure 32 the lower block has 2000 cycles and allows the complete decline of K_{PR} followed by steady state. The increase in the loading block leads to a gradual increase in K_{PR} according to the cycle dependent transition since the high loading cycles count as new overloads. After a certain number of cycles, the steady state K_{PR} of the high R value loading sequence is resumed and the next unloading cycle immediately lowers K_{PR} according to the master curve for constant amplitude loading.

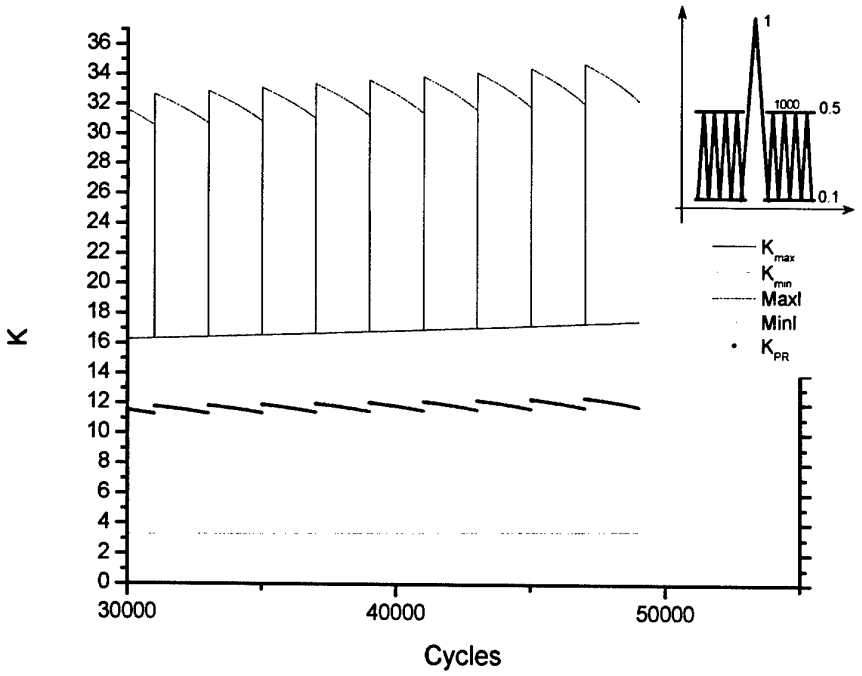

Figure 24

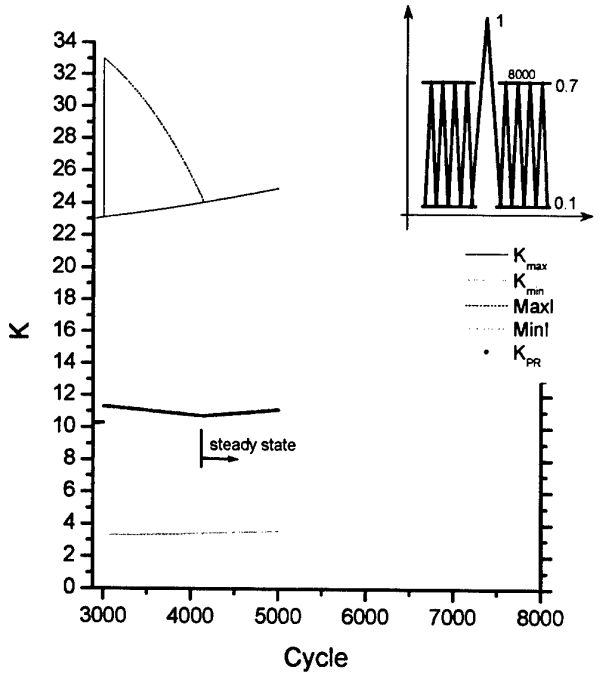

Figure 25

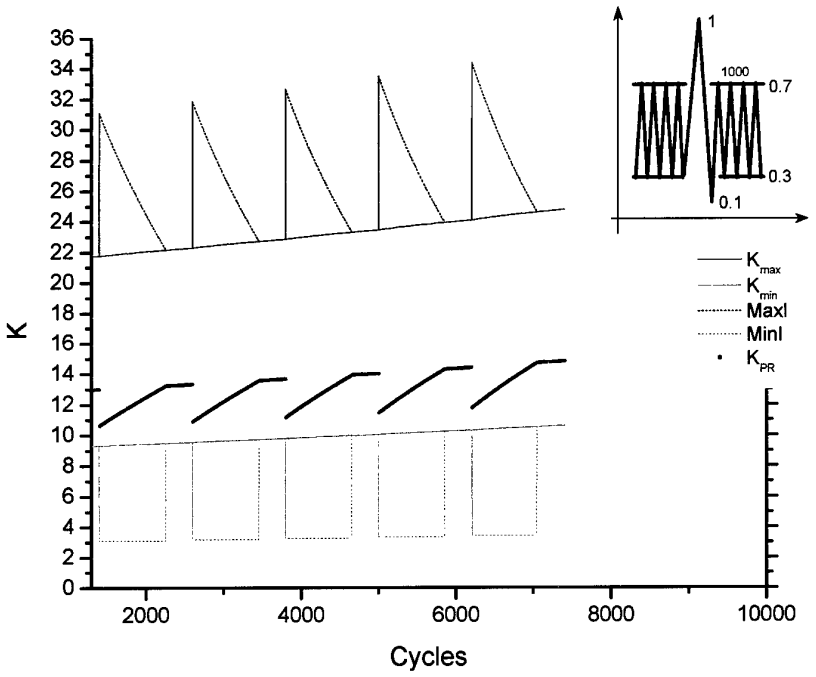

Figure 26

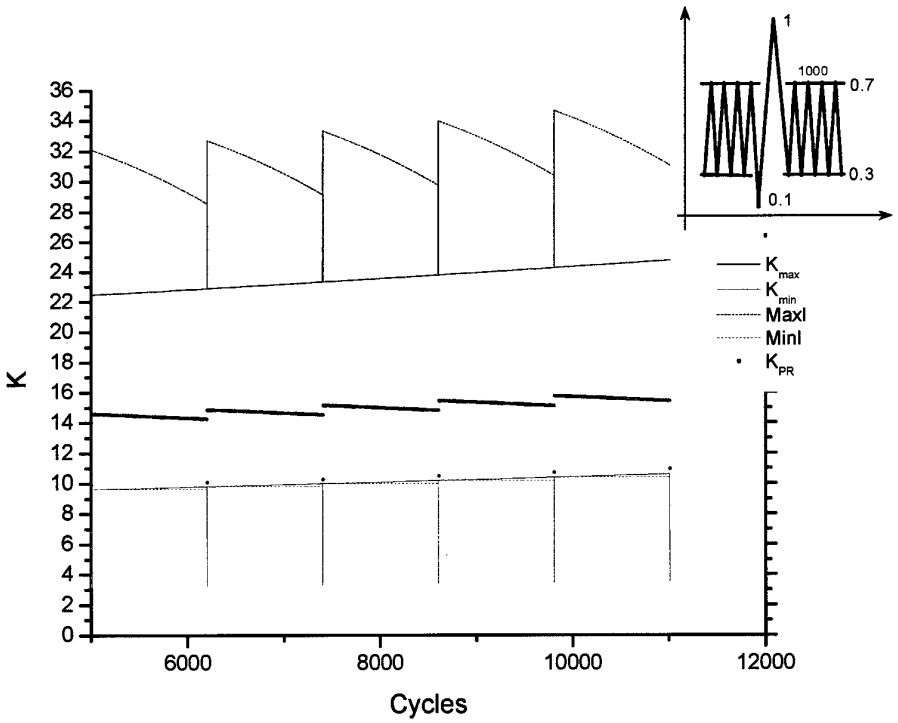

Figure 27

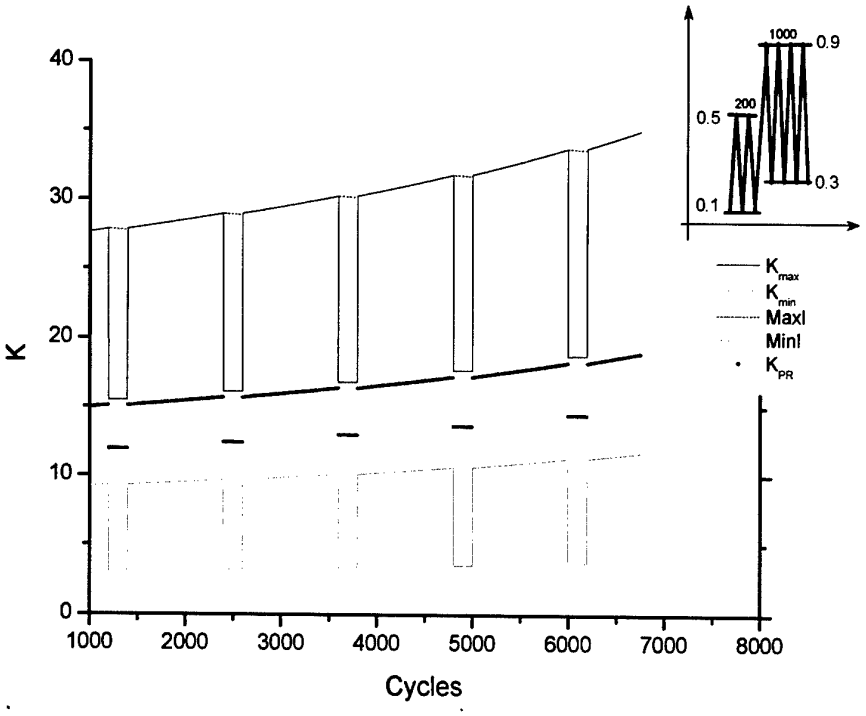

Figure 28

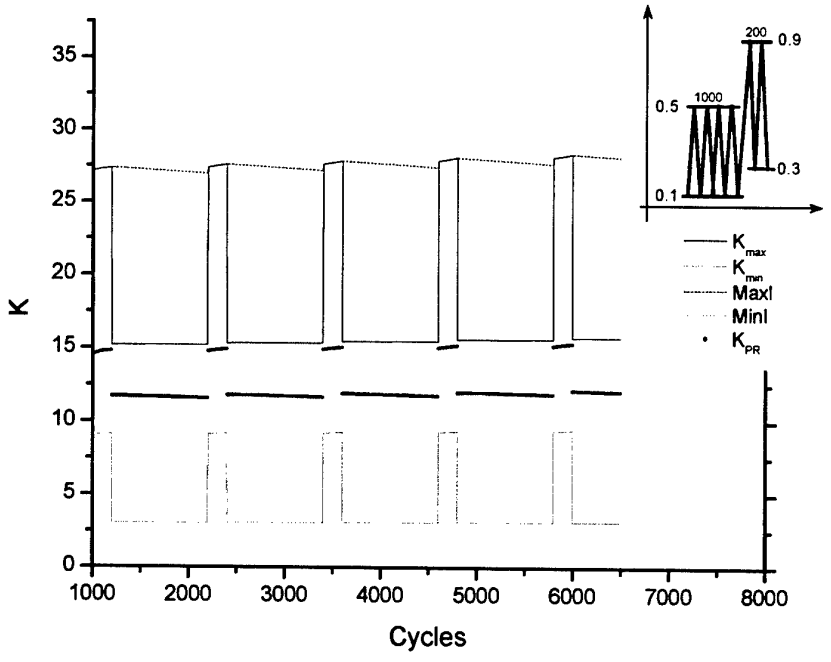

Figure 29

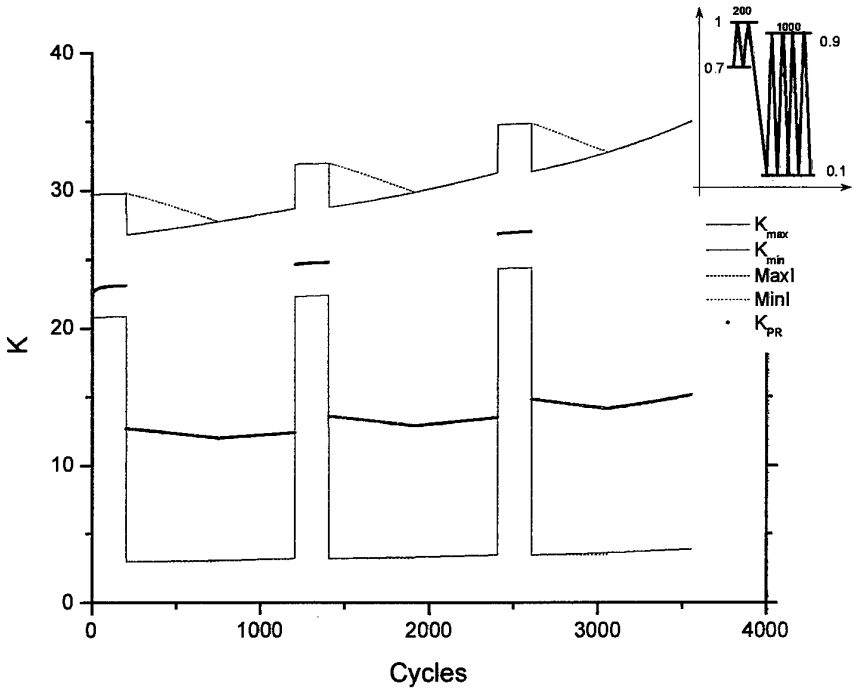

Figure 30

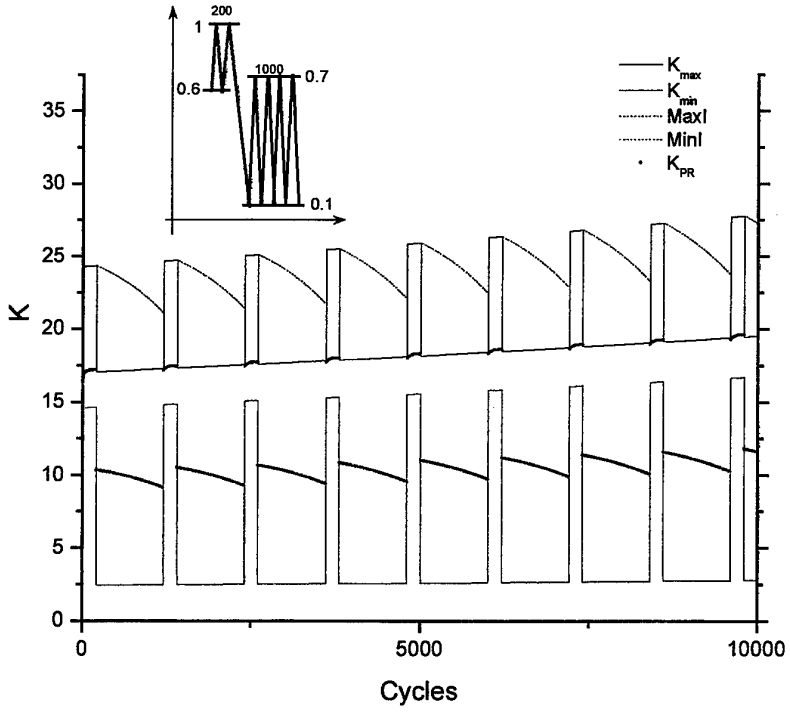

Figure 31

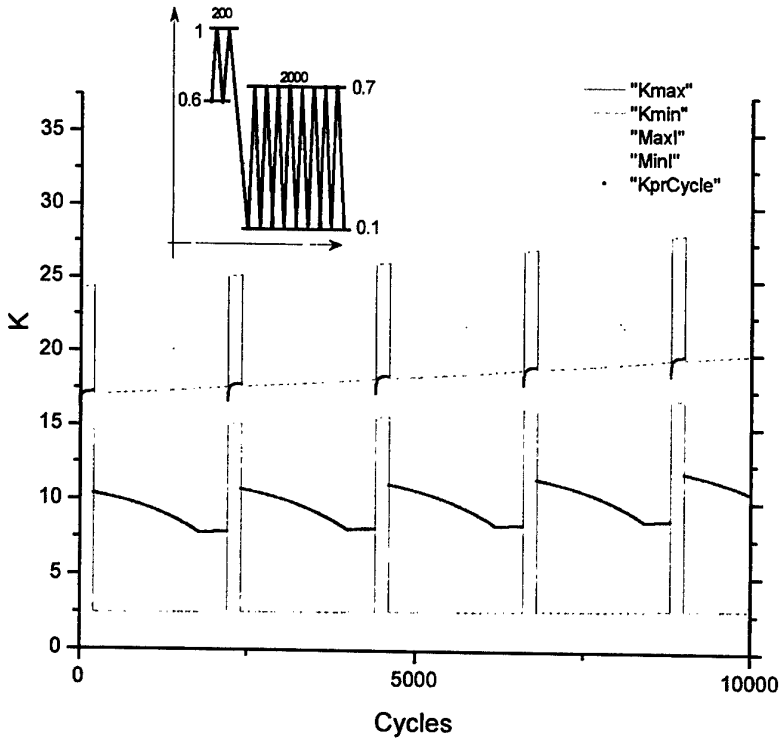

Figure 32

5.2 Model verification- comparison of predictions with experiment

5.2.1 Aluminium 7010, Rotarix Spectra

The evaluation of the K_{PR} model and the other four models was conducted using four different Rotarix spectra (Rotarix 16, 20, 24, 32) where the small cycles were omitted to a different degree. The Rotarix 16 spectrum is the largest spectrum and almost the original spectrum. The matrix is given below.

Test	Omission range level*	Rainflow cycle count in length	Reduction (%)
	Original Rot	1989925	---
1	16	1978108	0.6
2	20	113063	94.3
3	24	110907	94.4
4	32	51404	97.4

*Omission range level is the maximum cycle range retained.

The Rotarix 20 and 24 spectra are very similar. The nature of the spectrum used is typical for rotary wing structures. There is a large number of small cycles at high R-values along with a relatively low number of unloading cycles.

The blind predictions of the K_{PR} software are shown in Figure 33. The tests and the calculations were run on W = 70 mm, B = 17,5 mm CT (Compact Tension) specimen. The initial crack length and the loading condition along with the prediction results are listed in Table 21. The corresponding experimental results are listed in Table 22.

Table 21

K_{PR} Prediction Results

K_{PR} Pred. Al 7010	Max. Load	Initial crack length	K_{PR} – No Load Interaction		K_{PR} -Model		Diff. To Test	Div. To NoLIA
	[kN]	a [mm]	Cycles to Failure	Rotarix-loops to failure	Cycles to Failure	Rotarix-loops to failure		
Rotarix 16	10	15,9	10.271.267	5,19	6.441.012	3,26	2,00%	-37,29%
Rotarix 20	10	16,3	1.254.264	11,09	1.130.555	10	-12,70%	-9,86%
Rotarix 24	10	16,3	1.218.396	10,99	1.115.552	10,06	-13,90%	-8,44%
Rotarix 32	10	15,7	777.394	15,12	792.940	15,43	18,15%	2,00%

Table 22

TEST-Results Al 7010	Initial crack length	Test – Univ. Cranfield	
	a [mm]	Cycles to Failure	Rotarix-loops to failure
Rotarix 16	15,9	6.314.679	3,19
Rotarix 20	16,3	1.295.019	11,45
Rotarix 24	16,3	1.296.284	11,69
Rotarix 32	15,7	671.129	13,06

The difference between the calculations and the experimental results are indicated in Tables 21 and 22. The life of Rot 24 and 20 is almost the same, as was expected, and the Rotarix 16 spectrum leads to the longest life. Considering the number of cycles in one Rotarix loop, it becomes obvious that the omission level is of prime importance. In Figure 34 the results are plotted in terms of Rotarix loops (140 hours of flight). The Rotarix 16 spectrum needs only about three loops to failure, whereas the others need ten loops or more, showing that the majority of damage is due to level 16 cycles. The spectra with omission contain a greater proportion of unloading cycles in respect to the small high R rotor cycles.

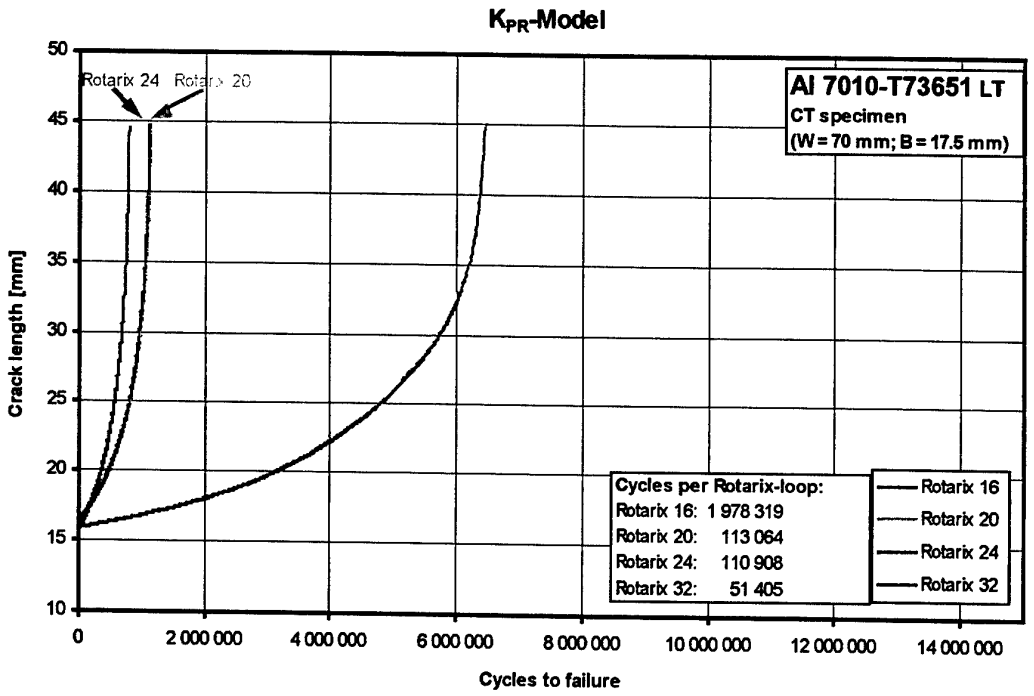

Figure 33: Predictions using the K_{PR} model; 7010 aluminium; Rotarix spectra

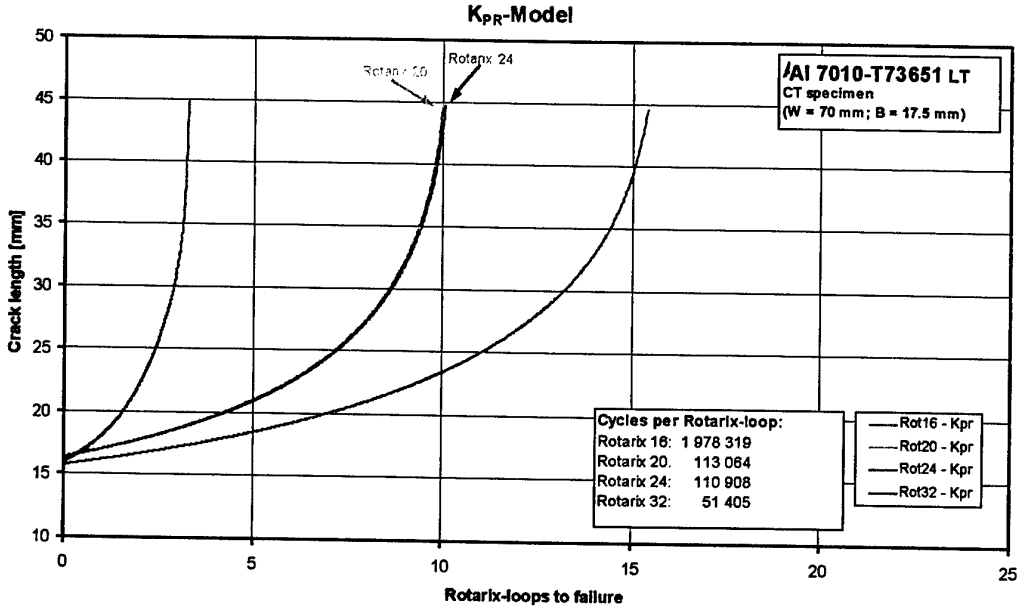

Figure 34: Predictions using the K_{PR} model 7010 aluminium; Rotarix spect

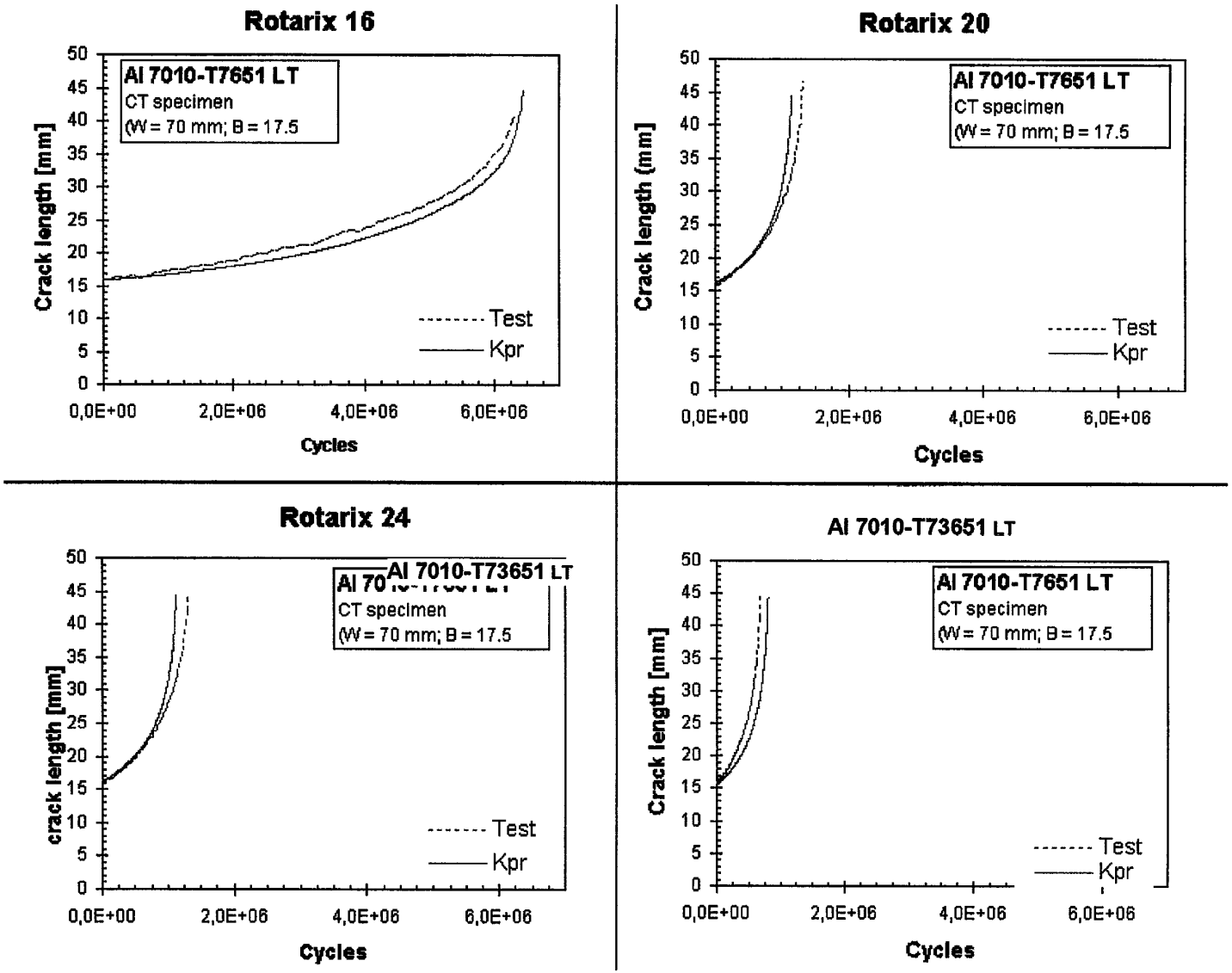

Figure 35: Comparison of K_{PR} Predictions and Test results; 7010 aluminium; Rotarix spectra

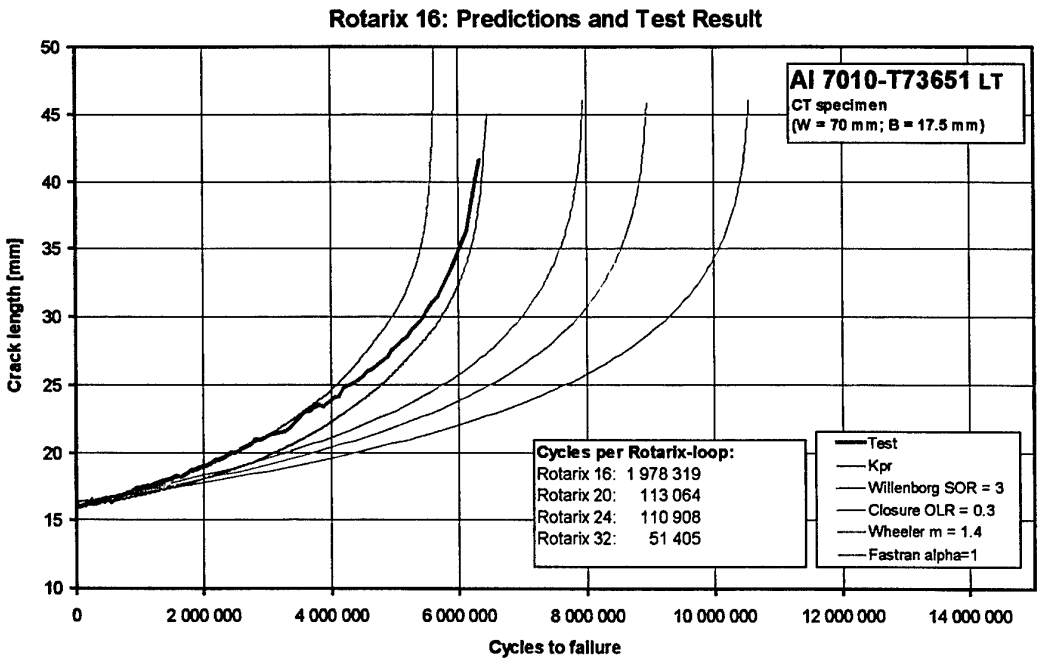

Figure 36: Comparison of the five different Models for Rotarix 16 (AFGROW using Forman fit) Rotarix spectra; 7010 aluminium

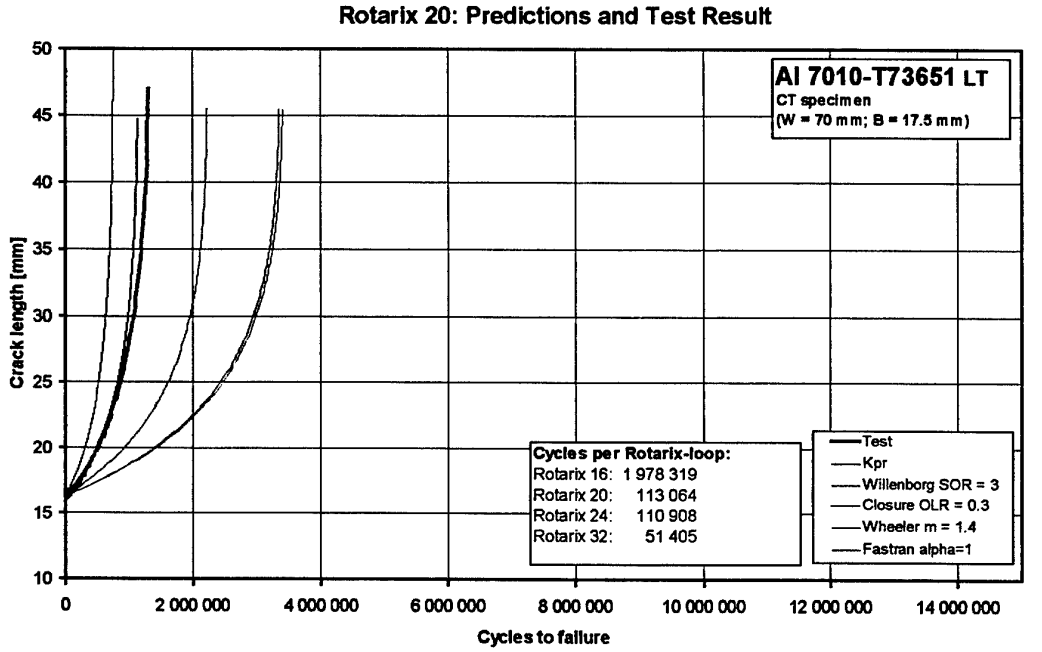

Figure 37: Comparison of the five different Models for Rotarix 20 (AFGROW using Forman fit); 7010 aluminium

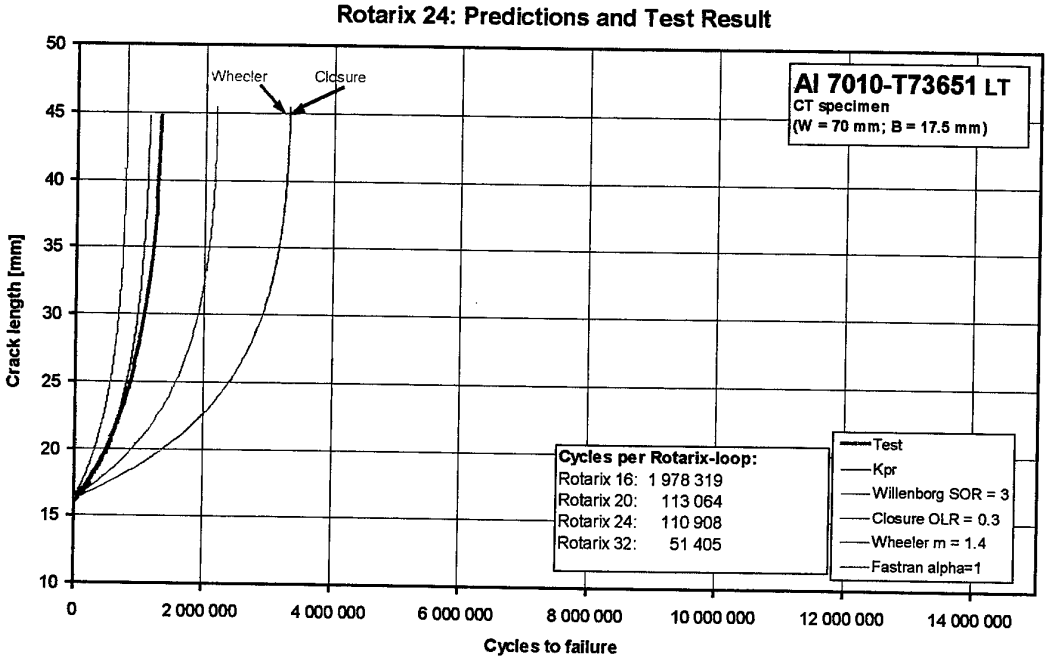

Figure 38: Comparison of the five different Models for Rotarix 24 (AFGROW using Forman fit); 7010 aluminium

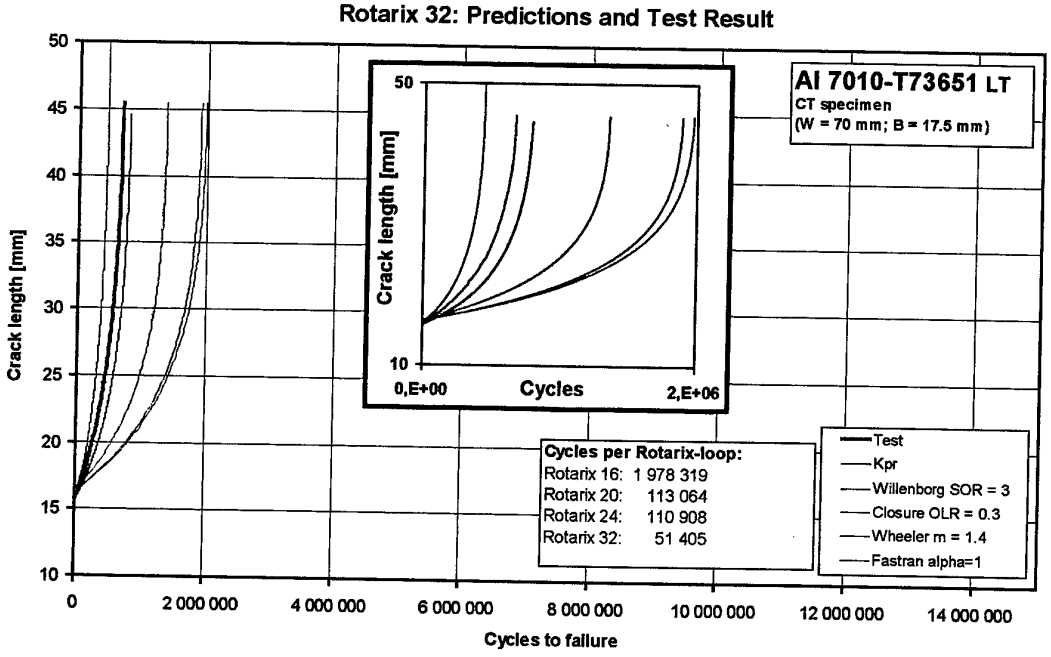

Figure 39: Comparison of the five different Models for Rotarix 32 (AFGROW using Forman fit); 7010 aluminium

The comparison of the test results with the predictions in Figure 35 give an excellent picture for the K_{PR} model. The percentage of the difference between test and predictions shown in Table 21

and ranges from –14% to + 18%. This difference is very small, compared to the prediction accuracy that can be expected today.

It needs to be emphasized that these were "blind" predictions. Cranfield University wanted to see the K_{PR} predictions first by the sub-contractor EADS - Military Aircraft, before the tests were conducted. The excellent result could well be a coincidence. However it does not seem that way since the K_{PR} software has no fitting parameter and all four spectra come out very well also in the shape of the crack growth curves. Also the other predictions were done blind. The fitting parameters for the other four models were chosen according to literature data or recommendations given in AFGROW manuals.

1) Wheeler model: m = 1.4 (9)
2) Willenborg model: SOR = 3 (according to AFGROW manual)
3) AFGROW Closure Model: OLR(@ R=0) = 0.3 (according to AFGROW manual)
4) FASTRAN Model: α= 1.

It has to be noted that in FASTRAN the constraint factor α is 1 for plane stress and 3 for plane strain. The constraint factor was chosen as 1 since this value collapsed the constant amplitude crack growth data best, which is the usual routine to fit the constraint to the crack growth data. The specimen used was with 17.5 mm thickness definitely a plain strain case and a factor towards 3 would be expected. A calculation with 2.5 or 3 however did not collapse the constant R da/dN data. A FASTRAN crack growth calculation with the pertaining plane strain factor would lead to shorter lives than shown here.

A comparison of all the models for the four spectra is shown in Figure 36 to Figure 39. FASTRAN and K_{PR} are the closest, where K_{PR} is nearer to the test result. FASTRAN is always conservative, and K_{PR} in two cases. The three other models yield unconservative results. The Willenborg model is closest to the test of these three and Closure and Wheeler are considerably unconservative. The exact numbers are given in Table 23.

Table 23

AFGROW Forman-Fit of all Data	Initial crack length	**Wheeler m=1.4**		**Willenborg SOR=3**		**Closure OLR=0.3**	
	a [mm]	Cycles to Failure	Rotarix-loops to Failure	Cycles to Failure	Rotarix-loops to Failure	Cycles to Failure	Rotarix-loops to Failure
Rotarix 16	15,9	8.947.217	4,52	7.953.156	4,02	10.545.279	5,33
Rotarix 20	16,3	3.400.174	30,07	2.220.487	19,64	3.354.057	29,67
Rotarix 24	16,3	3.259.334	29,39	2.164.920	19,52	3.308.313	29,83
Rotarix 32	15,7	1.892.451	36,81	1.356.924	26,40	1.976.250	38,44

Results FASTRAN	Initial crack length	α = 1	
	a [mm]	Cycles to Failure	Rotarix-loops to Failure
Rotarix 16	15,9	5.619.749	2,84
Rotarix 20	16,3	746.596	6,6
Rotarix 24	16,3	776.338	7,0
Rotarix 32	15,7	441.053	8,58

Helicopter spectra tend to have an acceleration effect rather than a retardation effect. To evaluate this behavior the crack growth lives without taking load interaction effects into account were calculated. The results are shown in Table 21 for the K_{PR} predictions and in Table 24 for AFGROW. It was not possible to do the same with FASTRAN. The respective crack growth data are displayed in Figures 40 –42. The crack growth lives without load interaction effects are longer than taking interaction into account, except for Rotarix 32. Compared with the test data, Rotarix 16 would be highly unconservative (over-predicted) if load interaction effects were excluded. Here we have a clear acceleration effect. For Rotarix 20 and 24 we see roughly the same results as in the test and also with Rotarix 32, almost the same life is calculated as in the test. It is assumed that acceleration and retardation effects equal each other to eventually come out as "unaffected." In the Rotarix 16 spectrum the large number of small cycles between the underload cycles allow the acceleration effect to stabilize over a longer region and more obviously effect the crack growth life. Forman was calculated without threshold and leads to shorter lives.

Table 24

AFGROW	Initial crack length	**Forman Fit**		**Tabular Input**	
No Load Interaction	a [mm]	Cycles to Failure	Rotarix-loops to failure	Cycles to Failure	Rotarix-loops to failure
Rotarix 16	15,9	7.971.561	4,03	9.927.589	5,02
Rotarix 20	16,3	2.219.242	19,63	1.843.266	16,30
Rotarix 24	16,3	2.163.490	19,51	1.789.519	16,14
Rotarix 32	15,7	1.353.553	26,33	1.097.665	21,35

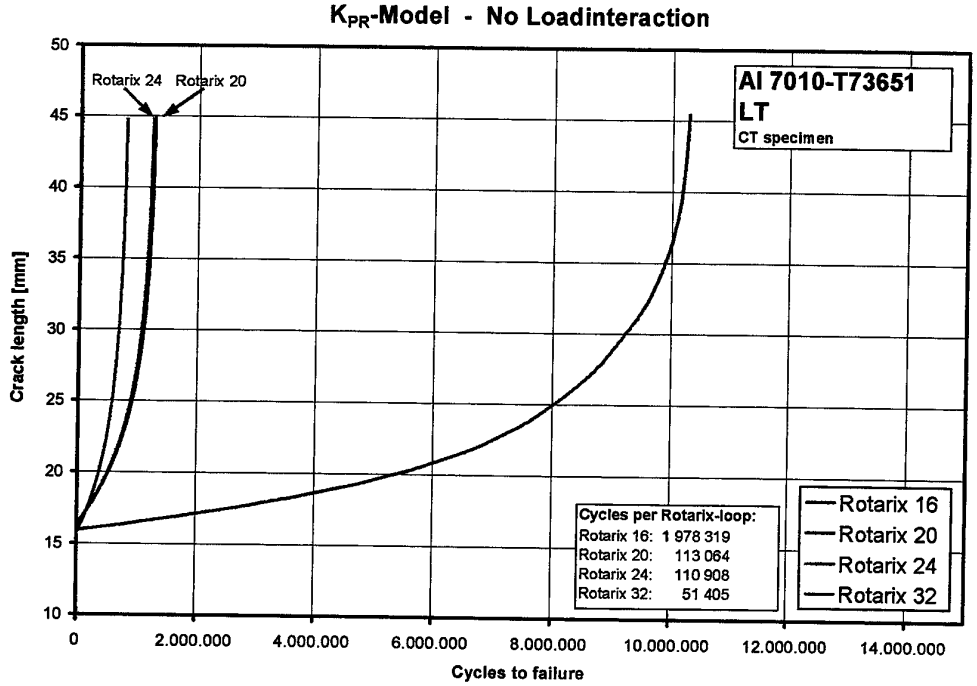

Figure 40 Comparison of K_{PR} predictions with no load iteration effects; 7010 aluminium; Rotarix spectra

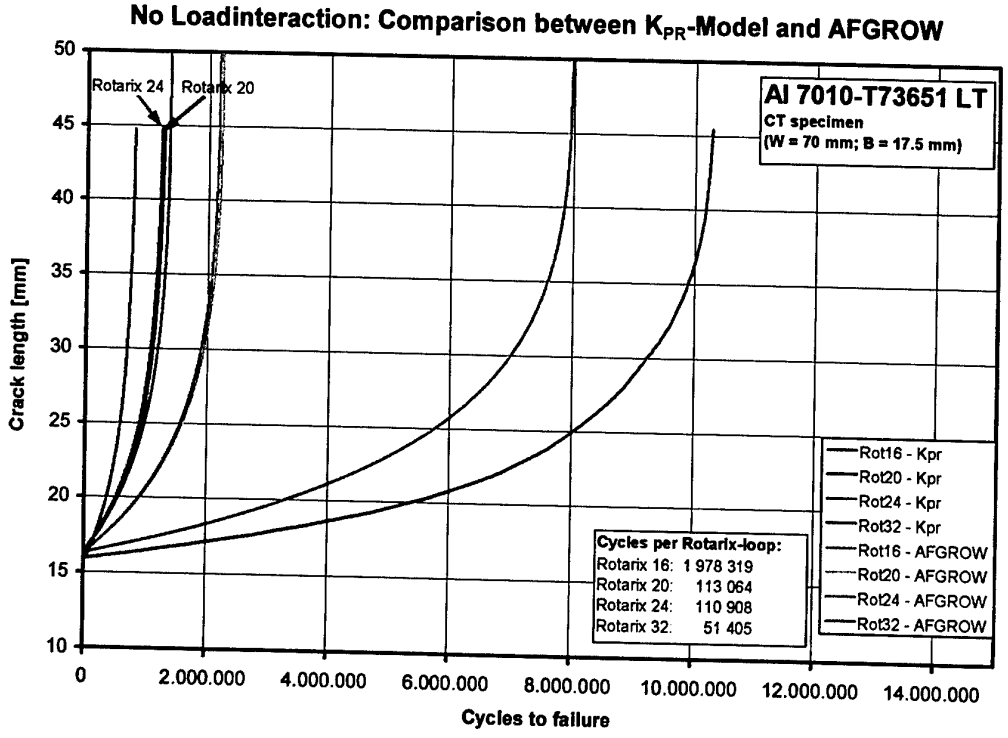

Figure 41 Comparison of K_{PR} and AFGROW (using Forman fit) predictions without Load Interaction Effects

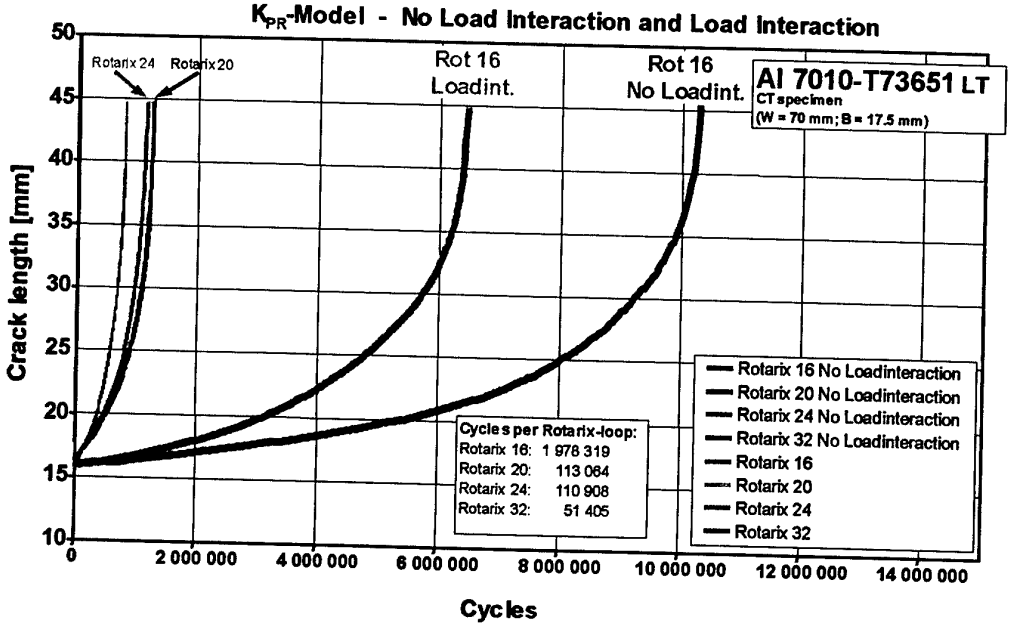

Figure 42

AFGROW predicts slight retardation and acceleration depending on the retardation model and the calculation of no-load interaction crack growth (Table 23, 24). The life with Rotarix 16 is 2% shorter than that with K_{PR}, but longer for all the other spectra.

A qualitative view as to whether the respective model itself predicts acceleration or retardation is possible. It has to be noted however that the calculations without load interaction effects are hard to be evaluated quantitatively since there is no experimental value for comparison, as load interaction effects are physically always there. The only way of judging the crack growth prediction capabilities without load interaction effects is to predict constant amplitude loading and compare with a test result. With this a clear understanding can be obtained of how well the crack growth data are represented in the model.

5.2.2 Comparison of K_{PR} predictions with test results for 4340 steel, Rotarix spectra

Data for testing and comparison for the 4340 steel were not as comprehensive as for the 7010 aluminium alloy. Comparisons were made under Rotarix 16 and Rotarix 32 spectra only. The results of the comparison between experiment and K_{PR} predictions for 4340 test data under Rotarix 16, together with AFGROW predictions for the 3 models is shown in Figure 43.

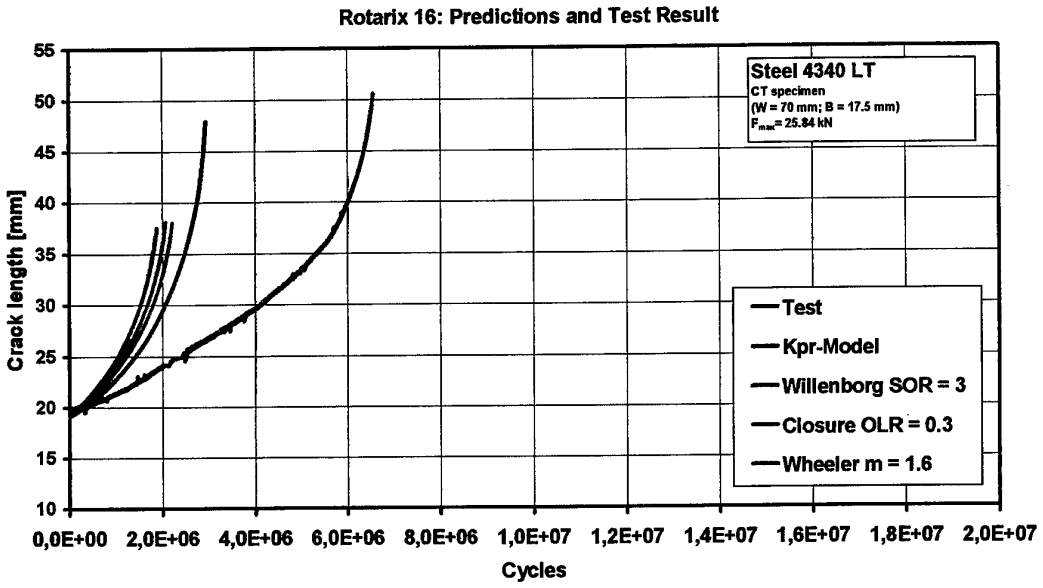

Figure 43 Comparison of test data for 4340 steel subjected to Rotarix 16 with K_{PR} predictions and AFGROW predictions

It will be seen that all the predicted lives are very conservative, by a factor of 3, with the K_{PR} model showing the most accurate result. However the total spread of predicted lives was about 15% of the experimental life of 6.5×10^6 cycles.

The same comparison for the much shorter Rotarix 32 spectrum is shown in Figure 44.

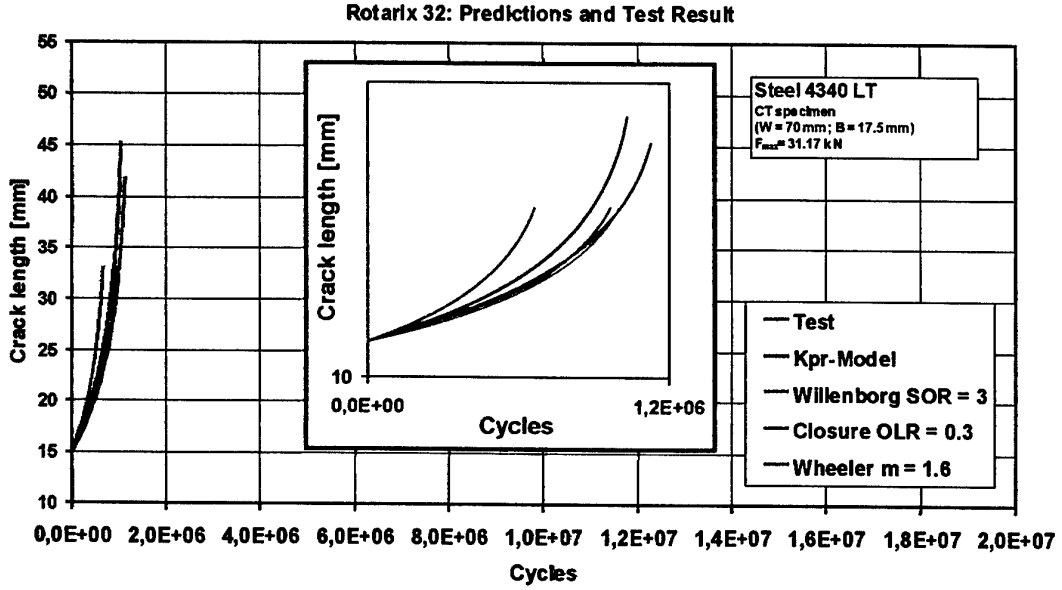

Figure 44 Comparison of Test data for 4340 steel subjected to Rotarix 32 spectrum, compared with predicted lives for AFGROW and for K_{PR}

Test lives in terms of cycles are of course considerably shorter for Rotarix 32. Once again the K_{PR} prediction was conservative with respect to the experimental life, but the most accurate prediction were the AFGROW Wheeler and closure models, with Willenborg being least accurate.

5.2.3 Comparison of experiment and predictions under Falstaff spectrum

Tests on 7010 aluminium

A limited number of tests were performed under the fighter wing spectrum Falstaff on both 7010 and 4340 materials. Experimental and predicted lives are shown in Figure 45 -47 for 7010 aluminium, tested under three different maximum test loads.

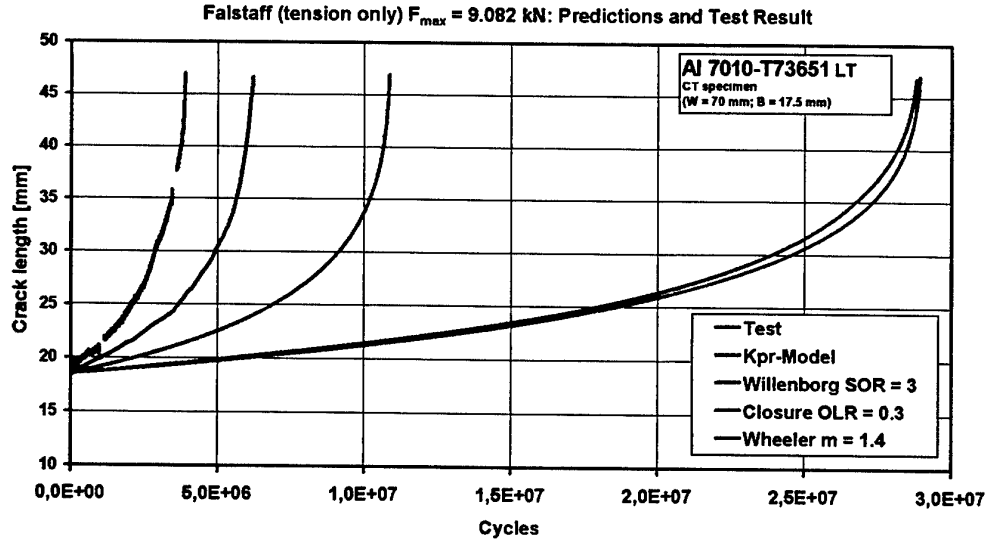

Figure 45 Comparison of experimental and predicted lives for K_{PR} and AFGROW models, 7010 under Falstaff spectrum. Peak load 9.082 kN.

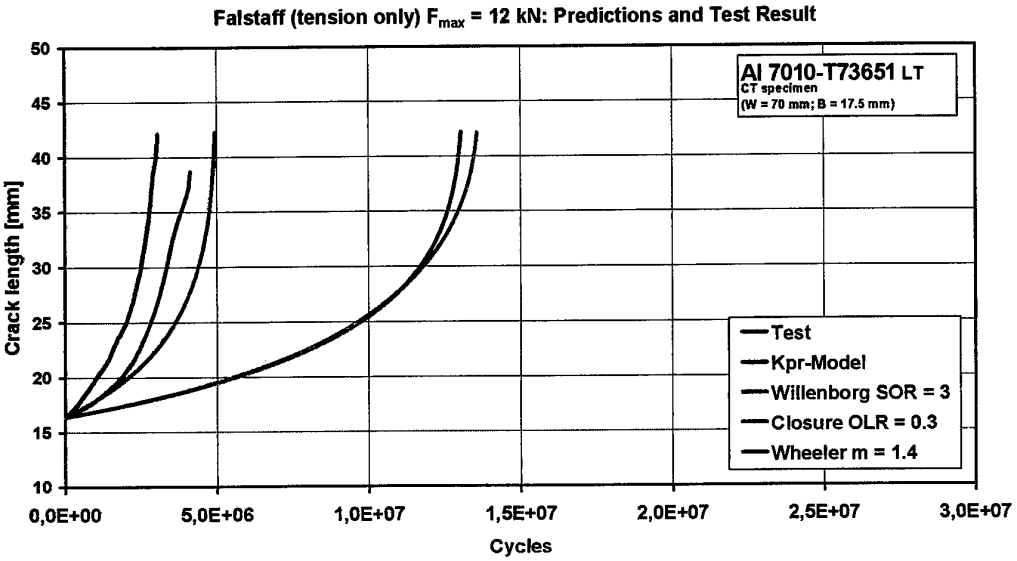

Figure 46 Comparison of experimental and predicted lives for K_{PR} and AFGROW models, 7010 under Falstaff spectrum. Peak load 12 kN

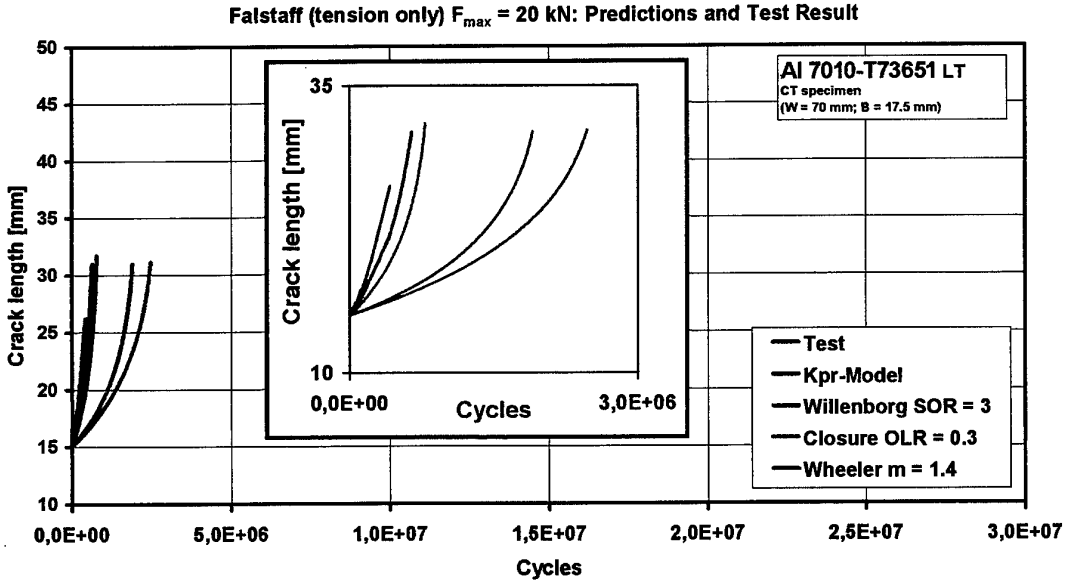

Figure 47 Comparison of experimental and predicted lives for K_{PR} and AFGROW models, 7010 under Falstaff spectrum. Peak load 20 kN

Figure 45 -47 show rather different rankings of the experimental data and the predictions. With 9 kN peak load, all predictions are non conservative, with the K_{PR} model being most accurate, followed by the three AFGROW models. With 12 kN peak load, the K_{PR} model was conservative with respect to the experimental data, with the other three models non conservative, and with approximately the same ranking. The K_{PR} error was 25-30%. The Willenborg model was just the most accurate, but was non conservative. With 20 kN the K_{PR} model gave the best result (slightly unconservative) followed by Willenborg.

Test on 4340 steel, Falstaff spectrum

A single test was conducted on 4340 steel under the Falstaff spectrum. The peak stress intensity was the same as was used as the peak for the Rotarix tests on 4340. Test results and predictions made using K_{PR} and the three AFGROW models are shown in Figure 48. It will be seen that the most accurate prediction is the Willenborg model, with all other predictions non conservative by a considerable margin. The K_{PR} model error was about a factor of three.

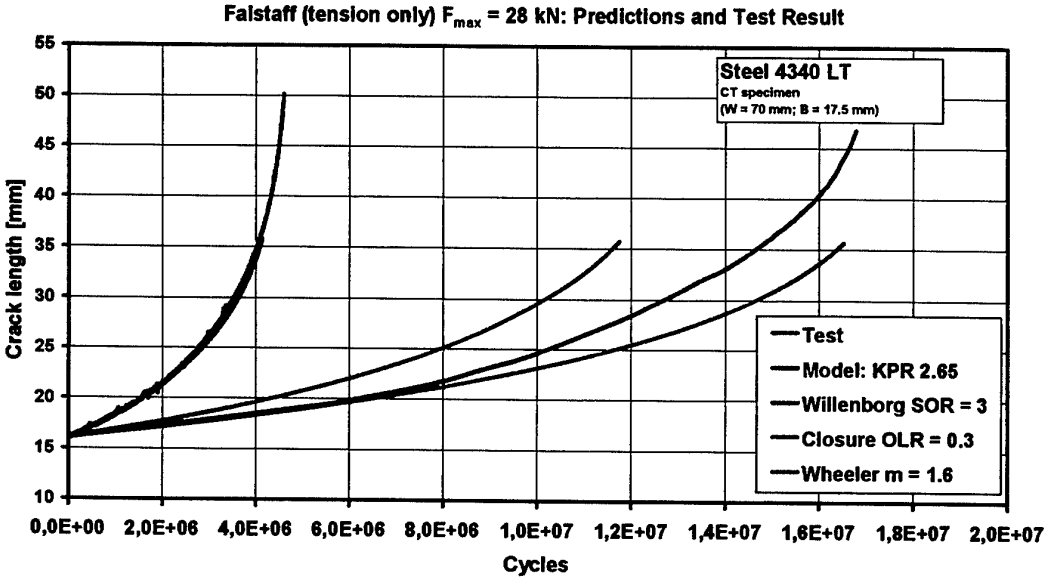

Figure 48 Comparison of test data for 4340 subjected to the Falstaff spectrum, with predictions for the three AFGROW models and the K_{PR} model.

6. Parameter study

To assess the variability of the models compared, the important parameters were varied. For the K_{PR} model eight different variations were conducted (denoted as Variation 1-10). The variation of the cycle dependent transition is shown in Figure 49. The difference in the result is very small, below 3% in all the spectra. This is understandable since there are not many consecutive overloads in the spectra.

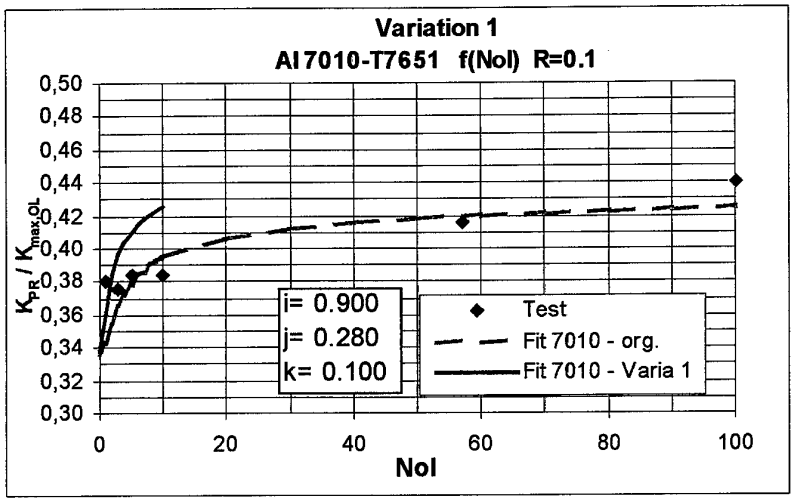

K_{PR}	Initial crack length	KPR - Mat 26 - Nolmax=100		KPR - Mat 26 V1 - Nolmax=10		Difference to Mat 26
	aC [mm]	Cycles to Failure	Rotarix-loops to failure	Cycles to Failure	Rotarix-loops to failure	in %
Rotarix 16	15,9	6.441.012	3,26	6.541.386	3,31	1,56%
Rotarix 20	16,3	1.130.555	10,00	1.162.516	10,28	2,83%
Rotarix 24	16,3	1.115.552	10,06	1.146.693	10,34	2,79%
Rotarix 32	15,7	792.940	15,43	804.739	15,65	1,49%

Figure 49

In Variation 2 the single overload Master Curve was taken the same as for CA loading. As can be seen in Figure 50, the predicted life of Rotarix 16 increases by 60 %. The overloads that occur after unloading and after high R-loading sequences cause now a high K_{PR} level, leading to a longer life. The Rotarix 20-32 spectra are not that affected since the periods of high R-loading between overloads are much smaller and thus an overload does not have the lasting effects as it has in Rotarix 16.

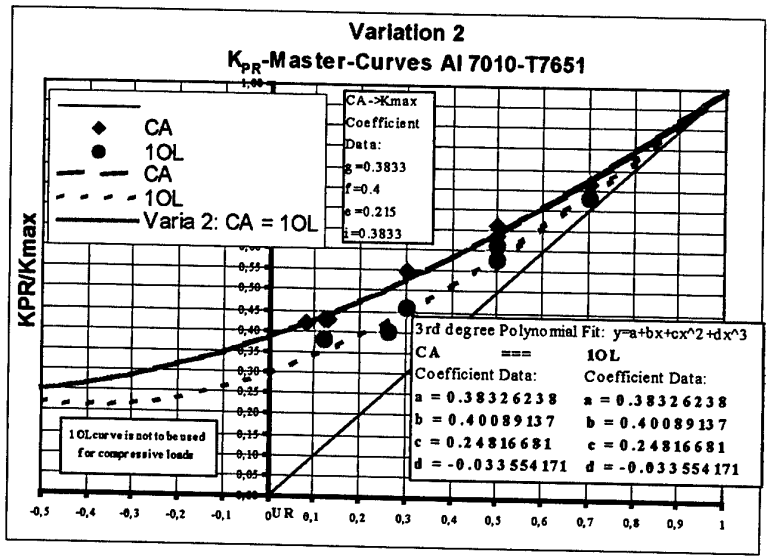

K_{PR}	Initial crack length aC [mm]	KPR - Mat 26		KPR - Mat 26 V2 - 1OL=CA		Difference to Mat 26 in %
		Cycles to Failure	Rotarix-loops to failure	Cycles to Failure	Rotarix-loops to failure	
Rotarix 16	15,9	6.441.012	3,26	10.344.039	5,23	60,60%
Rotarix 20	16,3	1.130.555	10,00	1.207.595	10,68	6,81%
Rotarix 24	16,3	1.115.552	10,06	1.190.185	10,73	6,69%
Rotarix 32	15,7	792.940	15,43	823.028	16,01	3,79%

Figure 50

In Variation 3 the single overload Master Curve was lowered (Figure 51). The life becomes shorter as expected. The quantitative effect is however only 15 % for Rot 16 and <3% for the other spectra. It needs to be noted that a spectrum that contains more overloads such as a fighter spectrum would be much more affected than a helicopter spectrum. The shift of the CA Master Curve would be of much more significance. This is shown in Variation 4 (Figure 52). The lives become 90 –155% longer compared to the actual material data. The sensitivity of the CA loading Master Curve in this spectrum is large, and it becomes important that the data to determine the CA loading Master Curve experimentally, are carefully obtained. The case where both the position of the CA loading Master Curve is raised and the single overload Master Curve is lowered is shown in Variation 5 (Figure 53). The lives become again smaller than in Variation 4, but as indicated in the related table in Figure 53, the change is very small such as the change in Variation 3. The variations involving the CA loading Master Curve are only an approximation. The crack growth curve and the CA loading Master Curve are attached to each other. The da/dN input is calculated due to the CA loading Master Curve. A change in the CA loading Master Curve is therefore only a first indication for the proportions of variability, but not a direct quantitative measure.

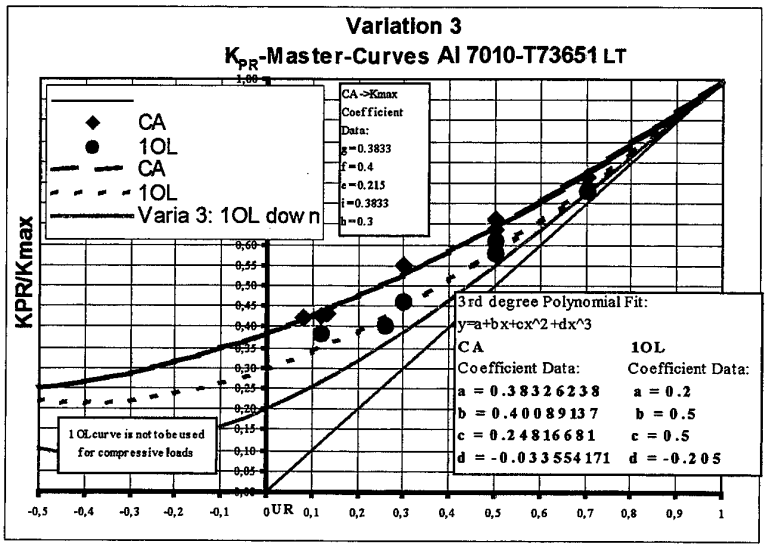

K_{PR}	Initial crack length	KPR - Mat 26		KPR - Mat 26 V3 - 1OL down		Difference to Mat 26
	aC [mm]	Cycles to Failure	Rotarix-loops to failure	Cycles to Failure	Rotarix-loops to failure	in %
Rotarix 16	15,9	6.441.012	3,26	5.502.074	2,78	-14,58%
Rotarix 20	16,3	1.130.555	10,00	1.100.390	9,73	-2,67%
Rotarix 24	16,3	1.115.552	10,06	1.086.451	9,80	-2,61%
Rotarix 32	15,7	792.940	15,43	774.350	15,06	-2,34%

Figure 51

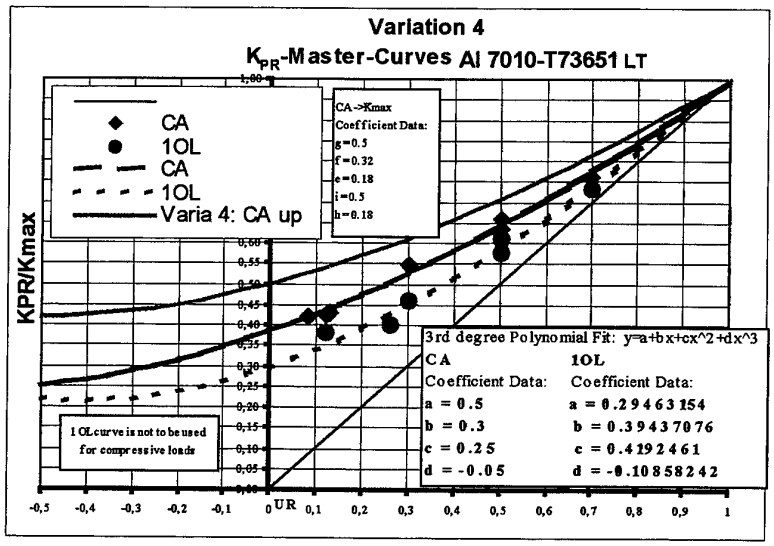

K_{PR}	Initial crack length	KPR - Mat 26		KPR - Mat 26 V4 - CA up		Difference to Mat 26
	aC [mm]	Cycles to Failure	Rotarix-loops to failure	Cycles to Failure	Rotarix-loops to failure	in %
Rotarix 16	15,9	6.441.012	3,26	12.138.430	6,14	88,46%
Rotarix 20	16,3	1.130.555	10,00	2.895.228	25,61	156,09%
Rotarix 24	16,3	1.115.552	10,06	2.858.590	25,77	156,25%
Rotarix 32	15,7	792.940	15,43	1.917.451	37,30	141,82%

Figure 52

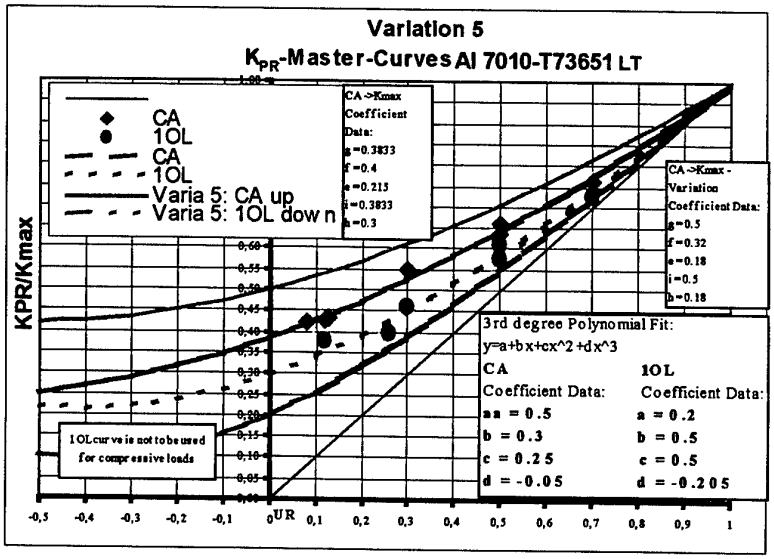

K_{PR}	Initial crack length	KPR - Mat 26		KPR - Mat 26 V5 - CA up + 1OL down		Difference to Mat 26
	aC [mm]	Cycles to Failure	Rotarix-loops to failure	Cycles to Failure	Rotarix-loops to failure	in %
Rotarix 16	15,9	6.441.012	3,26	10.667.206	5,39	65,61%
Rotarix 20	16,3	1.130.555	10,00	2.799.279	24,76	147,60%
Rotarix 24	16,3	1.115.552	10,06	2.765.551	24,94	147,91%
Rotarix 32	15,7	792.940	15,43	1.860.638	36,20	134,65%

Figure 53

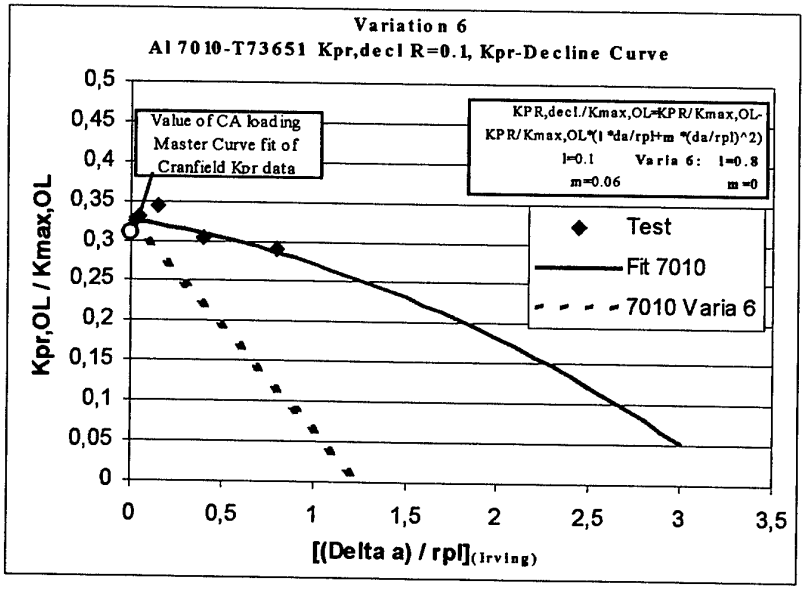

K_{PR}	Initial crack length	KPR - Mat 26		KPR - Mat 26 V6 - fast linear decline		Difference to Mat 26
	aC [mm]	Cycles to Failure	Rotarix-loops to failure	Cycles to Failure	Rotarix-loops to failure	in %
Rotarix 16	15,9	6.441.012	3,26	6.439.671	3,26	-0,02%
Rotarix 20	16,3	1.130.555	10,00	1.129.019	9,99	-0,14%
Rotarix 24	16,3	1.115.552	10,06	1.114.542	10,05	-0,09%
Rotarix 32	15,7	792.940	15,43	792.802	15,42	-0,02%

Figure 54

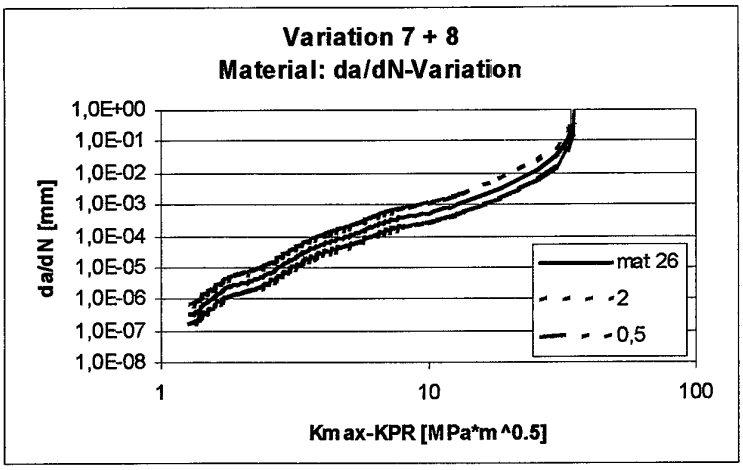

K_{PR}	initial crack length	KPR - Mat 26		KPR - Mat 26 V7 - da/dN*2		Difference to Mat 26
	aC [mm]	Cycles to Failure	Rotarix-loops to failure	Cycles to Failure	Rotarix-loops to failure	in %
Rotarix 16	15,9	6.441.012	3,26	3.209.444	1,62	-50,17%
Rotarix 20	16,3	1.130.555	10,00	559.776	4,95	-50,49%
Rotarix 24	16,3	1.115.552	10,06	552.390	4,98	-50,48%
Rotarix 32	15,7	792.940	15,43	393.972	7,66	-50,32%

K_{PR}	initial crack length	KPR - Mat 26		KPR - Mat 26 V8 - da/dN*0.5		Difference to Mat 26
	aC [mm]	Cycles to Failure	Rotarix-loops to failure	Cycles to Failure	Rotarix-loops to failure	in %
Rotarix 16	15,9	6.441.012	3,26	12.912.381	6,53	100,47%
Rotarix 20	16,3	1.130.555	10,00	2.284.629	20,21	102,08%
Rotarix 24	16,3	1.115.552	10,06	2.253.795	20,32	102,03%
Rotarix 32	15,7	792.940	15,43	1.590.278	30,94	100,55%

Figure 55

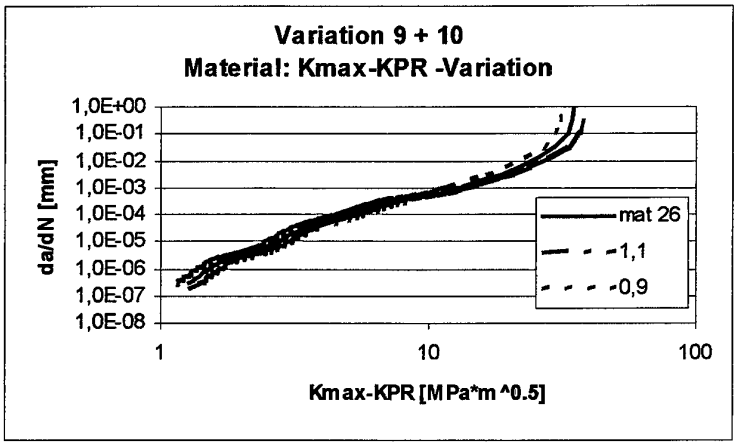

K_{PR}	initial crack length	KPR - Mat 26		KPR - Mat 26 V9 - Kmax-KPR*1.1		Difference to Mat 26
	aC [mm]	Cycles to Failure	Rotarix-loops to failure	Cycles to Failure	Rotarix-loops to failure	in %
Rotarix 16	15,9	6.441.012	3,26	10.334.116	5,22	60,44%
Rotarix 20	16,3	1.130.555	10,00	1.659.117	14,67	46,75%
Rotarix 24	16,3	1.115.552	10,06	1.637.300	14,76	46,77%
Rotarix 32	15,7	792.940	15,43	1.151.170	22,39	45,18%

K_{PR}-2.64	initial crack length	KPR - Mat 26		KPR - Mat 26 V10 - Kmax-KPR*0.9		Difference to Mat 26
	aC [mm]	Cycles to Failure	Rotarix-loops to failure	Cycles to Failure	Rotarix-loops to failure	in %
Rotarix 16	15,9	6.441.012	3,26	4.090.355	2,07	-36,50%
Rotarix 20	16,3	1.130.555	10,00	752.996	6,66	-33,40%
Rotarix 24	16,3	1.115.552	10,06	742.601	6,70	-33,43%
Rotarix 32	15,7	792.940	15,43	541.815	10,54	-31,67%

Figure 56

In Variation 6 (Figure 54) the decline curve was lowered to yield a quicker recovery of K_{PR} after an overload. The effect is almost negligible. The model is designed such that K_{PR} after an overload is lowered towards the steady state K_{PR} value at the end of the respective plastic zone of the respective following cycle. The changes in Variation 6 therefore only change the shape of the decline curve, but do not really shorten the period over which K_{PR} declines, even though it seems to be the case considering the green curve in Figure 54.

Variation 7 and 8 are trivial. A shift in the crack growth rate by a factor of 0.5 and 2 was conducted leading to a 50% and 200% change in life. This example only shows that the crack growth curve algorithm is programmed correctly.

Variation 9 and 10 are somewhat similar to Variation 4. Here it is not the CA loading Master Curve that is altered, but changes are made at the other end, at the crack growth curve, as if the shift from ΔK to $K_{max} - K_{PR}$ was done with a different CA loading Master Curve. The da/dN data were shifted horizontally by ± 10%. The life does not change proportionally between the different spectra. It changes most for the Rotarix 16 spectrum, and there for the case of +10%. This can be explained by the fact that a linear shift has more influence on the lower K_{max}-K_{PR} values of about 1-3 MPa $m^{1/2}$ than between 10-20 MPa $m^{1/2}$, as can be seen in 56. Rotarix has proportionally more cycles in the lower effective range region (more smaller cycles) than Rotarix 20-32 with the increasing omission level.

7. Final Comments

The excellent agreement of the K_{PR} model with variable amplitude crack growth tests for 7010 aluminium under the helicopter rotorhead Rotarix spectrum is extremely encouraging. The approach is relatively new and novel in terms of the physical description of fatigue crack growth and the material properties which are required for its operation. On all 4 variants of the Rotarix spectrum, life errors of 2-15% were found. This is excellent accuracy, particularly when set against the 100% errors and more produced by AFGROW model variants. FASTRAN was the most accurate of the other models investigated. The greatest errors in predictions of K_{PR} were found in Rotarix 32, a spectrum which has an increased overload content compared to the tensile underloads which are found in the Rotarix 16 spectrum. It was still more accurate than other models.

The Falstaff spectrum is characterised by overloads rather than underloads, and in this spectrum, K_{PR} performed less well with errors of 30-50% on the 7010 aluminium alloy. All the models tended to over predict (non conservative errors) the experimental lives. FASTRAN was the most accurate for the low K_{max} 7010 test and was comparable with Willenborg in the higher Kmax test, K_{PR} made a conservative prediction in the latter. This aspect of the prediction capability of K_{PR} is deserving of closer study. The difference in K_{PR} response in overloads spectra as opposed to underload spectra is something treated by different aspects of the model. It may be that better definition of repeated overload behaviour would improve the accuracy still further, although once again it should be emphasised that even at its worst, on 7010 alloy, K_{PR} was the most accurate. It has to be emphasized that the predictions were blind. Considering the large errors, known from blind predictions, the errors in the K_{PR} predictions are very encouraging and the approach seems to be a prediction improvement.

The least successful performance of the model was on the 4340 steel. On Rotarix 16 and 32 spectra, the errors were a factor of 2 (100%) non conservative, and 20% conservative. On Rotarix 16 K_{PR} was still the most accurate model; on Rotarix 32 AFGROW Closure and Wheeler were both highly accurate with negligible error. Under the Falstaff spectrum, K_{PR} had a non

conservative error of a factor of three, and AFGROW Willenborg and Closure models were better than it. It is suspected that the crack growth data were inadequately characterised in this material (few crack growth data and not large scatter, see Figures 22 and 23). It has already been noted that the crack growth master curve, plotting da/dN against $K_{max} - K_{PR}$ did not completely collapse the data. It would be worth re visiting predictions on this material with better characterisation of its crack growth behaviour to see if the predictions turn out improved.

Considering the relatively recent debut and relative lack of maturity of the K_{PR} approach, the performance described in this report is extremely promising. The FASTRAN model performed almost as well, and it is interesting to note that they both use a ΔK_{eff} approach in which ΔK_{eff} is calculated on a cycle by cycle basis, although the estimation of ΔK_{eff} is performed using very different approaches. It is somewhat confusing that FASTRAN came out mostly conservative even with a plain stress constraint factor ($\alpha = 1$), while the specimen is predominantly a plain strain case. A physically appropriate constraint factor of plain strain ($\alpha = 2,5 - 3$) would however yield even shorter lives.

The procedure of automated testing techniques for accurate measurement of K_{PR} material parameters, as has been realized in this research, makes the approach a practical reality. Much more K_{PR} material data are required and once gathered, are available for use on future occasions. The extent of applicability of these concepts in terms of material type- high strength or low strength, ductile or brittle, high modulus or low modulus requires establishing. Also, the interaction of the K_{PR} properties with different types of loading history would be a valuable source of insights.

Besides the ability to predict crack growth, the K_{PR} approach opens new phenomenological views and new possibilities in damage tolerance applications for design of structures. For example, the positions of the two master curves (Fig. 12-15) is of prime importance for the damage tolerance of a material. It is favourable when the curves are high in respect to the ratio of K_{PR}/K_{max}. If the master curves are far apart, the overloads have a relatively moderate retardation effects. However, here the yield strength is important too, since in case it is low, the cyclic plastic zone is larger promoting retardation that lasts longer compared to the opposite case. The curves are further apart for 4340 steel than in 7010 aluminium, but the absolute position of the curves in 4340 is higher. Therefore the damage tolerance of 4340 is higher than of 7010.

The crack growth rates are an additional important factor here, which are also lower in 4340 (compare Figures 20 and 23). Especially ΔK_T and its correct determination is important here. The parameter study in section 6 indicates that not the material itself is determining the property of "damage tolerance," but also the type of spectra involved, meaning the application, is of high importance. It is for example better for helicopter and turbine engine materials to have a high constant amplitude master curve, while the emphasis for a material in a fighter fuselage or lower wing skin material would be to have a high single overload master curve. For an engine application it is best to have both curves high and narrow together (underloads as in helicopters and dispersed small overloads), as is the case for Ti-6242 (13). Not yet published work has shown that the master curves also change with temperature, where they spread apart with increasing temperature. We know already since a long time from practical experience that damage tolerance is not only a structures and material property, but also depends on other parameters such as the type of spectra involved or the temperature of operation. The K_{PR} approach is able to reflect and explain these aspects, which is a very good sign for a sound physical basis of a crack growth model.

The authors think that is will be possible in a foreseeable time to evaluate structural material applications in terms of the K_{PR} approach and recommend the right material for a specific application. The right choice of a material is a mix of the right position of the master curves, ΔK_T,

yield strength and the crack growth rates, to have best performance for the respective application and spectra (leaving out mere static properties and corrosion considerations for a moment). We have an equation with a few parameters to be combined to an optimum to yield the right material for a given damage tolerance application. First ideas exist to form a damage tolerance parameter that reflects these properties for major classifications of spectra (helicopter, engines, fighter, etc.), which could be taken into account by designers when trading the different static, corrosion, weight and fatigue properties of application of materials in structures development. These abilities of the K_{PR} approach go beyond the mere question whether the model predicts fatigue crack growth better or worse than other prediction models.

8. Conclusions

8.1 An automated computer controlled fatigue test system using a DC potential drop system for crack length monitoring, greatly facilitates the measurement of K_{PR} values under constant amplitude loading, after single overloads, after multiple overloads and at increasing distances after the application of an overload.

8.2 The equipment has been used to measure K_{PR} on 7010 T73651 aluminium and in SAE 4340 quenched and tempered steel. The values obtained are broadly in agreement with previous measurements of this type on other aluminium alloys. K_{PR}/K_{max} values were significantly greater in the SAE 4340 steel than in the aluminium alloy.

8.3 Fatigue crack growth data at constant R and at constant K_{max} has been measured for both the aluminium and the 4340 steel. These data in conjunction with K_{PR} data gathered after constant amplitude loading, have been used to derive a ΔK_{eff} vs da/dN curve for the two materials. The ΔK_{eff} collapsed the data for a range of R ratios very well for 7010, less well for the 4340.

8.4 Predictions using the K_{PR} model of crack growth fatigue lives under the Rotarix helicopter test spectra, showed excellent agreement with experimental lives measured on the same test spectra. Errors of 2-20% were found.

8.5 Predictions under the same conditions, made using Wheeler, Willenborg and closure based models within AFGROW produced non conservative predictions with large errors. Predictions based on FASTRAN had errors slightly bigger than those found for K_{PR}.

8.6 Predictions of crack growth lives for the fighter wing spectrum Falstaff on 7010 aluminium, showed greater errors of up to 50% although K_{PR} predictions were still the most accurate of the models tested. Predictions made of crack growth lives on SAE 4340 steel under Rotarix and Falstaff spectra showed non conservative errors of a factor of two for Rotarix 16 and errors of a factor of 3 under the Falstaff spectrum. The only situation where K_{PR} predictions were not the most accurate of the models or nearly the best was for 4340 steel under Falstaff. This result may be associated with lack of comprehensive crack growth data for the 4340 material, a problem that should be revisited with more accurate crack growth data.

9. References

(1) Irving, P E. Buller, R G. (1998). Prediction of Fatigue Life Under Helicopter Loading Spectra for Safe Life and Damage Tolerant Design, in *Fatigue and Fracture Mechanics, 29th Volume, ASTM STP 1321,* Eds T L Panotin, S D Sheppard, ASTM.

(2) Buller, R G. Irving, P E. (1997). Experimental Investigation of Small Cycle Omission Levels in Helicopter Loading Spectra, in *ICAF'97,* Edinburgh, June, Pub EMAS, 1998; pp 441-460.

(3) Cook, R. Graaskov, D. Chilton A. (1998). Robust crack growth model for rotorcraft metallic structures. Final report on DTI contract RA/6/30/06.

(4) Lang, M. (2000). A model for fatigue crack growth, Part I: Phenomenology, *Fat. & Fracture of Engng. Mat. & Str.*, Vol. 23, 587-601.

(5) Lang, M. (2000). A model for fatigue crack growth, Part II: Modelling, *Fat. & Fracture of Engng. Mat. & Str.*, Vol. 23, 603-617.

(6) Lang, M. (1999). Description of load interaction effects by the ΔK_{eff} concept. In *Advances in fatigue crack closure measurement and analysis ASTM STP 1343 ASTM West Conshohocken PA USA* pp 207-223.

(7) Lang, M. Marci, G. "Reflecting on the mechanical driving force of fatigue crack propagation," ASTM STP 1321, *Vol 29,* 1998, pp. 474-495.

(8) Lang, M. Huang, X. "The influence of compressive loads on fatigue crack propagation, in metals", Fatigue & Fracture of Engng. Materials & Structures, Vol. 21,No. 1, 1998, pp. 65 – 84.

(9) Broek, D. Smith, S H. The prediction of fatigue crack growth under flight-by-flight loading, engineering fracture mechanics, Vol. 11, pp. 123-141, 1979.

(10) Lang, M. Huang, X (1998). The influence of compressive loads on fatigue crack propagation. *Fatigue Fract. Eng. Mater. Struct.* **21** pp 65-83.

(11) van Dijk, G M. de Jonge, J B (1975). Introduction to a fighter loading standard for fatigue evaluation: Falstaff, NLR MP 75017 U.

(12) Edwards, P R. Darts, J. (1984). Standardised fatigue loading sequences for helicopter Rotors (Helix and Felix) Reports RAE TR -84084 and TR-84085.